
Pattern wavelengths and transport characteristics in three-dimensional bioconvection generated by chemotactic bacteria

A PREPRINT

 **Hideki Yanaoka** *

Department of Systems Innovation Engineering,
Faculty of Science and Engineering, Iwate University,
4-3-5 Ueda, Morioka1, Iwate 202-8551, Japan

Tomomu Nishimura

Kawasaki Heavy Industries, Ltd.,
1-14-5 Kaigan, Minato-ku, Tokyo 105-8315, Japan

4 July 2022

ABSTRACT

We conducted a three-dimensional numerical simulation of bioconvection generated by oxygen-reactive chemotactic bacteria. This study investigated the bioconvection patterns, interference between plumes, and the wavelength of bioconvection patterns. In addition, we clarified the transport characteristics of cells and oxygen in the bioconvection. Multiple plumes occur in the suspension and three-dimensional bioconvection is formed around the plumes by the cells with vortex rings arising around the plumes. Even if bioconvection at a high Rayleigh number is disturbed, the bioconvection is strongly stable with respect to disturbances, and the pattern does not change due to disturbances. Bioconvection changes depending on the physical properties of bacteria and oxygen, and, in particular, the rate of oxygen consumption by bacteria significantly affects the strength of bioconvection. Bioconvection patterns with different plume arrangements and shapes are formed for different Rayleigh numbers or initial disturbances of the cell concentration. As a result, the wavelengths of the patterns also vary. As the Rayleigh number increases, interference between plumes is strengthened by the shortening of the pattern wavelength, so the velocities of both upward and downward flows increase. Many cells are located under the plumes and a strong shear flow occurs in these regions. As the pattern wavelength decreases, the cells are affected by high shear stress. Then, the convective transport of the entire suspension strengthens and the transport characteristics of cells and oxygen improve. When the chamber boundary is changed to side walls, bacteria adhere to the wall surface, and plumes are regularly arranged along the side walls.

1 Introduction

Microorganisms inhabit the Earth in a vast variety of environments (Omori et al., 2003). Some of these microorganisms respond to outside stimuli and move in selected directions. These responses are called taxis. Taxis responding to gravity, light, and chemicals are respectively called gravitaxis, phototaxis, and chemotaxis. In suspension, when a certain quantity of microorganisms accumulates near a free surface due to taxis, cells of the microorganisms fall, and thus bioconvection is generated (Platt, 1961) because the cells are denser than water (Hart and Edwards, 1987).

Many studies have been made on bioconvection (Pedley and Kessler, 1992; Hillesdon et al., 1995; Hillesdon and Pedley, 1996; Bees and Hill, 1997; Metcalfe and Pedley, 1998; Czirók et al., 2000; Ghorai and Hill, 2002; Metcalfe and Pedley, 2001; Yanaoka et al., 2007, 2008; Williams and Bees, 2011; Chertock et al., 2012; Kage et al., 2013; Karimi and Paul, 2013). Microorganisms have been used for environmental cleanup in various fields (Omori et al., 2002; Hirooka and Nagase, 2003; Omori et al., 2003). Bioconvection can be applied to driving micromechanical systems (Itoh et al., 2001, 2006), mixing chemicals (Geng and Kuznetsov, 2005), detecting toxicity (Noever and Matsos, 1991a,b; Noever et al., 1992), controlling microorganisms in biochips, as well as other applications. Furthermore, the production of biofuels by microorganisms has attracted attention from the viewpoint

*Email address for correspondence: yanaoka@iwate-u.ac.jp

of being clean and environmentally friendly. [Bees and Croze \(2014\)](#) discussed the possibility that microorganisms with taxis may be able to mix biofuel-producing microorganisms efficiently. Therefore, for the efficient utilization of microorganisms in various fields, it is important to determine the behavior of microorganisms and the mass transfer characteristics in bioconvection generated by microorganisms with taxis.

Regarding bioconvection generated by chemotactic bacteria responding to oxygen, theoretical ([Hillesdon and Pedley, 1996](#); [Metcalf and Pedley, 1998, 2001](#)), experimental ([Pedley and Kessler, 1992](#); [Hillesdon et al., 1995](#); [Czirók et al., 2000](#)), and numerical studies ([Yanaoka et al., 2007, 2008](#); [Chertock et al., 2012](#); [Lee and Kim, 2015](#)) have been conducted. However, earlier numerical studies were two-dimensional analyses or three-dimensional analyses on a single plume with a fixed wavelength ([Yanaoka et al., 2007, 2008](#)). Hence, it was not possible to capture complicated three-dimensional phenomena that multiple plumes exhibit in the chamber. Although basic studies on the wavelength of bioconvection patterns have been carried out ([Bees and Hill, 1997](#); [Czirók et al., 2000](#); [Ghorai and Hill, 2002](#); [Karimi and Paul, 2013](#)), no studies have been reported on the influences of wavelength variations on the transport characteristics and interference between plumes.

Studies on the control of bioconvection have been performed to utilize microorganisms for engineering purposes ([Itoh et al., 2001, 2006](#); [Kuznetsov, 2005](#)). Furthermore, various studies have been conducted on nano-bioconvection in suspensions containing nanoparticles and bacteria ([Kuznetsov, 2011](#); [Geng and Kuznetsov, 2005](#); [Uddin et al., 2016](#); [Zadeha et al., 2020](#)). Recently, bioconvection in suspensions containing microorganisms and nanoparticles under an applied magnetic field has been investigated ([Naseem et al., 2017](#); [Khan et al., 2020](#); [Shi et al., 2021](#)). New applicative research on bioconvection is underway. However, in the previous studies, the phenomenon of three-dimensional bioconvection has not been captured because a stability analysis was performed or the fundamental equations were solved by similarity transformation. Bioconvection with multiple microbial plumes is complex, and the details of the transport characteristics in bioconvection have not been clarified.

Bioconvection is a three-dimensional phenomenon and multiple plumes will exist in a chamber. Under such circumstances, the plumes interfere with each other and the accompanying change in the wavelength of the bioconvection pattern affects the transport characteristics. From the above viewpoints, we simulate three-dimensional bioconvection generated by oxygen-reactive chemotactic bacteria, and then clarify the bioconvection patterns, interference between plumes, the wavelengths of each pattern, and the transport characteristics of cells and oxygen when multiple plumes arise.

2 Numerical Procedures

Figure 1 shows the flow configuration and coordinate system. A suspension in a chamber contains bacterial cells, and the depth of the suspension is h . The origin is at the bottom wall of the chamber. The x - and y -axes are in the horizontal and vertical direction, respectively, and the z -axis is in the direction perpendicular to the page.

We assume that the suspension is sufficiently dilute for hydrodynamic cell-cell interactions to be negligible, and consider an incompressible viscous fluid. The fundamental equations are the continuity equation, the momentum equation under the Boussinesq approximation, and the conservation equations for cells and oxygen ([Hillesdon et al., 1995](#); [Hillesdon and Pedley, 1996](#)), given as

$$\nabla \cdot \mathbf{u} = 0 \quad (1)$$

$$\frac{\partial \mathbf{u}}{\partial t} + \nabla \cdot (\mathbf{u} \otimes \mathbf{u}) = -\frac{1}{\rho} \nabla p + \nu \nabla^2 \mathbf{u} + \frac{gnV(\rho_n - \rho)\mathbf{e}}{\rho} \quad (2)$$

$$\frac{\partial n}{\partial t} + \nabla \cdot (\mathbf{u}n + \mathbf{V}n - \mathbf{D}_n \nabla n) = 0 \quad (3)$$

$$\frac{\partial c}{\partial t} + \nabla \cdot (\mathbf{u}c - D_c \nabla c) = -Kn \quad (4)$$

where t is time, \mathbf{u} is flow velocity, p is pressure, ρ and ν are the density and kinematic viscosity of the fluid, respectively, ρ_n is the density of the cell, V is the volume of a cell, g is the gravity acceleration, $\mathbf{e} = -\hat{\mathbf{y}}$ is the unit vector in the direction of gravity, n is cell concentration, c is oxygen concentration, \mathbf{V} is the average cell swimming velocity, \mathbf{D}_n is the cell diffusivity tensor, D_c is the oxygen diffusivity, and K is the rate of oxygen consumption by cells.

In this study, the swimming of microorganisms is modelled similarly to that of [Hillesdon et al. \(1995\)](#). [Berg and Brown \(1972\)](#) found that the swimming velocity of microorganisms has both directional and random components. The random swimming of the cell is modelled as cell diffusion. The cell diffusion is assumed to be isotropic and the cell diffusivity tensor \mathbf{D}_n is modelled as $\mathbf{D}_n = D_{n0}H(c^*)\mathbf{I}$. Here, c^* is the non-dimensional oxygen concentration, $H(c^*)$ is a step function, and \mathbf{I} is the identity tensor. c^* is defined as $c^* = (c - c_{\min})/(c_0 - c_{\min})$, where c_0 is the initial oxygen concentration, and c_{\min} is the minimum oxygen concentration required for the cell to be active. Next, the directional

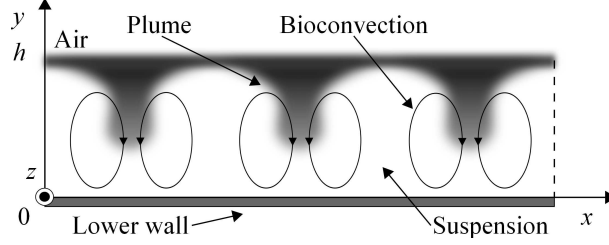


Figure 1: Flow configuration and coordinate system

swimming of the cell is modelled as an average swimming velocity. The average cell swimming velocity vector \mathbf{V} is modelled as being proportional to the oxygen concentration gradient and is defined as $\mathbf{V} = bV_s H(c^*) \nabla c^*$. The oxygen consumption rate K by cells is modelled as $K = K_0 H(c^*)$ like that of Hillesdon et al. (1995). Here, D_{n0} , b , V_s , and K_0 are constants. In this study, $H(c^*)$ is modelled with an approximate equation, $H(c^*) = 1 - \exp(-c^*/c_1^*)$, to suppress discontinuous changes due to the step function (Hillesdon et al., 1995). Here, c_1^* is 0.01 (Hillesdon et al., 1995; Yanaoka et al., 2007, 2008). Hillesdon et al. (1995) investigated the effect of c_1^* on the concentration distribution in a stationary field, and the qualitative trend did not change. In the present study, c_1^* is set to a small value. Therefore, in a shallow chamber treated in the present study, since oxygen is transported to the bottom, the step function $H(c^*)$ is approximately 1.0, and the modelling of $H(c^*)$ does not affect the calculation results.

A non-slip boundary condition is set at the bottom wall and the gradients perpendicular to the wall are to be assumed zero for the cell and oxygen concentrations. At the free surface, a slip boundary condition is imposed for the velocity field, the flux of cell concentration is zero, and the oxygen concentration is constant. Further, periodic boundary conditions are imposed in the x - and z -directions for the velocity and concentration fields.

The variables of the fundamental equations are non-dimensionalized in the same way as in previous studies (Hillesdon et al., 1995; Yanaoka et al., 2007, 2008) as follows.

$$\mathbf{x}^* = \frac{\mathbf{x}}{h}, \quad \mathbf{u}^* = \frac{\mathbf{u}}{D_{n0}/h}, \quad p^* = \frac{p}{\rho(D_{n0}/h)^2}, \quad t^* = \frac{t}{h^2/D_{n0}}, \quad n^* = \frac{n}{n_0}, \quad (5)$$

where the superscript $*$ represents a non-dimensional variable, and n_0 is the initial cell concentration. Thus, the non-dimensional fundamental equations are written as

$$\nabla \cdot \mathbf{u}^* = 0 \quad (6)$$

$$\frac{1}{Sc} \left[\frac{\partial \mathbf{u}^*}{\partial t^*} + \nabla \cdot (\mathbf{u}^* \otimes \mathbf{u}^*) \right] = -\nabla p^* + \nabla^2 \mathbf{u}^* + Ra n^* \mathbf{e} \quad (7)$$

$$\frac{\partial n^*}{\partial t^*} + \nabla \cdot \left[\mathbf{u}^* n^* + H(c^*) \gamma n^* \nabla c^* - H(c^*) \nabla n^* \right] = 0 \quad (8)$$

$$\frac{\partial c^*}{\partial t^*} + \nabla \cdot (\mathbf{u}^* c^* - \delta \nabla c^*) = -H(c^*) \delta \beta n^* \quad (9)$$

where the non-dimensional parameters are given by equation (10). The parameter β represents the strength of oxygen consumption relative to its diffusion, γ is a measure of the relative strengths of directional and random swimming, and δ is the ratio of oxygen diffusivity to cell diffusivity. Ra is the Rayleigh number and Sc is the Schmidt number.

$$\beta = \frac{K_0 n_0 h^2}{D_c (c_0 - c_{\min})}, \quad \gamma = \frac{bV_s}{D_{n0}}, \quad \delta = \frac{D_c}{D_{n0}}, \quad Ra = \frac{V n_0 g h^3 (\rho_n - \rho)}{\nu D_{n0} \rho}, \quad Sc = \frac{\nu}{D_{n0}} \quad (10)$$

The governing equations are solved using the SMAC method (Amsden and Harlow, 1970). This study uses the Euler implicit method for the time differentials and the second-order central difference scheme for the space differentials.

3 Calculation conditions

This study considers chemotactic bacteria responding to oxygen as microorganisms with taxis, and investigates the characteristics of three-dimensional bioconvection in the chamber. As the initial condition, the suspension is stationary, and the cell and oxygen concentrations are constant. Similar to the previous study (Ghorai and Hill, 2002), low

initial disturbances are added to the cell concentration in the suspension to model the initial state in an experiment of bioconvection. The initial concentration is defined as

$$n = n_0 [1 + \varepsilon A(x, y)] \quad (11)$$

where $\varepsilon = 10^{-2}$ and $A(x, y)$ is a random number generated in the range of -1 to 1 . The random number is generated by the Mersenne twister method (Matsumoto and Nishimura, 1998) and the initial value is given by the linear congruent method. To investigate the stability of bioconvection with respect to disturbance, we use the obtained calculation result as an initial condition.

The x - and z -dimensions of the computational region are set to $10h$. To clarify the effect of the length of the calculation area on the formation of bioconvection, we also performed a calculation for the calculation area $L = 20h$. This study used four uniform grids of $91 \times 31 \times 91$ (grid1), $101 \times 51 \times 101$ (grid2), $111 \times 81 \times 111$ (grid3), and $141 \times 101 \times 141$ (grid4) for $L = 10h$ to examine the grid dependency of the numerical results. We confirmed that the grid resolution of grid2 was suitable for obtaining valid results, so the results of grid2 are shown in the following. In the calculation for $L = 20h$, we used a uniform grid of $201 \times 51 \times 201$, which has the same resolution as grid2.

Non-dimensional parameters are given using the properties of *Bacillus subtilis* that responds to oxygen gradients. The diffusion coefficient of bacteria D_{n0} is different in each study, and the range is 10^{-6} to 10^{-5} cm^2/s (Hillesdon et al., 1995; Hillesdon and Pedley, 1996; Tual et al., 2005). This study takes $D_{n0} = 10^{-5}$ cm^2/s and adopts values for the other properties from Hillesdon et al. (1995) and Hillesdon and Pedley (1996). Therefore, the non-dimensional base parameters are $\beta = 1$, $\gamma = 2$, $\delta = 2$, and $Sc = 1000$. We change some base parameters to investigate the effects of the physical properties of bacteria and oxygen on bioconvection. The calculation was conducted for eight different Rayleigh numbers, $Ra = 0, 250, 500, 1000, 2000, 3000, 4000$, and 5000 . The bioconvection occurs above the critical Rayleigh number. Variations of the bioconvection patterns and the wavelengths depending on the initial condition have been observed in earlier experimental research (Bees and Hill, 1997). At $Ra = 500$ and 5000 , greater than the critical Rayleigh number, we have investigated whether the same tendency as the experimental result is observed for 10 kinds of initial disturbance to the cell concentration. The results for all Rayleigh numbers are convergent solutions and represent steady-state flow and concentration fields.

4 Numerical results and discussion

4.1 Comparison with the theoretical solution

The present numerical result is compared with the linear theoretical solution (Hillesdon et al., 1995) to confirm its validity. The theoretical value is a solution for a shallow chamber. Figure 2 shows the cell and oxygen concentration distributions in the y -direction for $Ra = 0, 250$, and 500 . Here, the cross-section are at $x/h = 5.0$, $z/h = 5.0$ for $Ra = 0$ and $Ra = 250$, and $x/h = 5.9$, $z/h = 4.1$ at the centre of the plume for $Ra = 500$. The plume is shown below in figures 4 and 5. We define the plume centre as the position where the cell concentration on the free surface is maximum. These calculation results for $Ra = 0, 250$ agree well with the theoretical solution. However, it is confirmed that a large difference appears between the result at $Ra = 500$ and the theoretical result, suggesting the occurrence of bioconvection, which is a non-linear phenomenon. The previous study (Yanaoka et al., 2008) showed that bioconvection occurs at a Rayleigh number greater than the critical number. In this study, since bioconvection occurs at $Ra = 500$, it is considered that the critical Rayleigh number lies between $Ra = 250$ and 500 .

4.2 Occurrence of bioconvection

First, we investigate the occurrence of bioconvection when the Rayleigh number is changed. Figures 3 and 4 show the flow and concentration fields for $Ra = 250, 500$. At $Ra = 250$, the bacterial cells are concentrated near the water surface because they react with the oxygen supplied from the water surface and move upward due to chemotaxis. As the fluid is almost stationary and is not transported by convection, the oxygen concentration distribution is two-dimensional. The oxygen concentration decreases from the water surface to the lower wall. From above, because the suspension is stable up to $Ra = 250$ and bioconvection does not occur, it is considered that the critical Rayleigh number is at $Ra > 250$. In the cell concentration field of $Ra = 500$ shown in figure 4 (a), high-concentration cells concentrated near the water surface settle toward the lower wall at $x/h = 3.3$. This falling region of cells is called a plume, and this result suggests the occurrence of bioconvection. As shown in figure 4 (d), the plumes form in a staggered manner, so the cross-section of $z/h = 6.5$ is located across one plume. Therefore, in figure 4 (a), the influence of one plume appears significantly. Still, even around $x/h = 7.0$ and 9.5 , the cell concentration is distorted by the influence of the surrounding plumes. Slight fluctuations are observed in the oxygen concentration distribution, and weak convection occurs in the velocity vector. In the oxygen concentration field for $Ra = 500$, because the Rayleigh number is low, the effect of diffusion is greater than that of convection. In the cell concentration field, even if

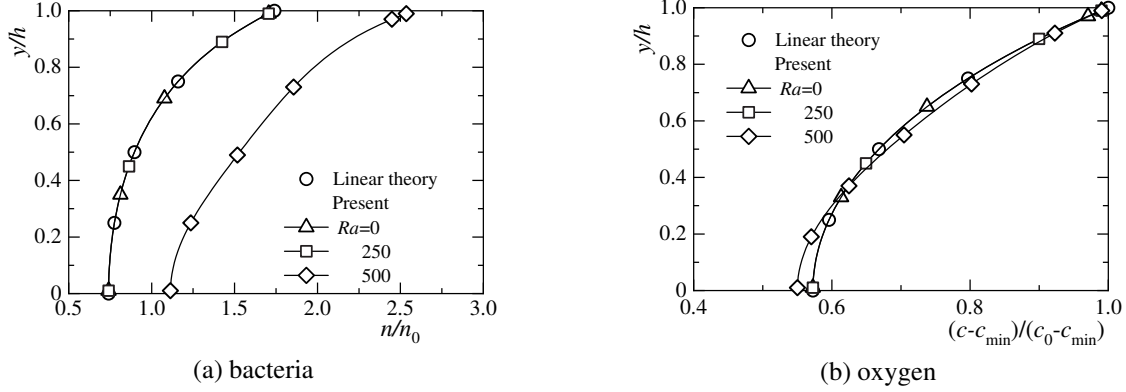


Figure 2: Comparison of concentration distributions with linear theoretical solution (Hillesdon et al., 1995).

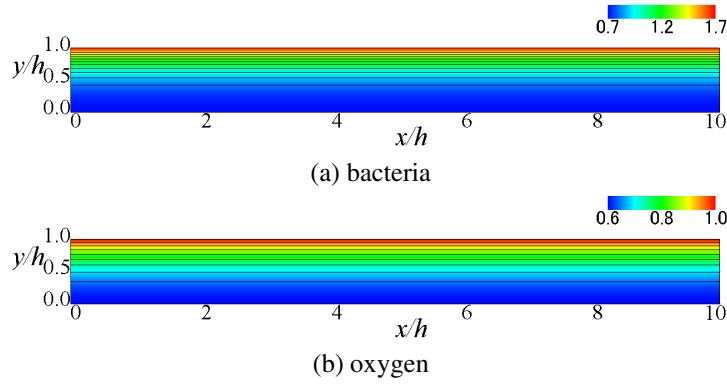


Figure 3: Bacterial and oxygen concentration contours for $Ra = 250$ at $z/h = 5.0$.

the Rayleigh number is low, transport by directional swimming works in addition to random swimming, so the effect of convection becomes large. Since bacteria consume oxygen, oxygen consumption increases in the plume, where the cell concentration is high. Therefore, the oxygen concentration does not have a distribution similar to the cell concentration. We can see from figure 2 that the oxygen concentration for $Ra = 500$ is similar to that for $Ra = 250$. The effect of the interference between bacteria and oxygen appears in the oxygen concentration distribution.

When $\beta = 0$, bacteria do not consume oxygen. We calculated the condition of $\beta = 0$ at $Ra = 500$, and bioconvection did not occur. The suspension became a uniform concentration field. This result suggests that oxygen consumption due to bacteria causes interference between bacteria and oxygen, forming bioconvection. Bioconvection is similar to the Rayleigh–Bénard convection. However, the properties of microorganisms and their interaction with oxygen determine the stability of the suspension and convection pattern. Chemotactic bacteria respond to the oxygen gradient and consume oxygen. Therefore, the bacteria themselves create an oxygen gradient. As the bacteria move, the oxygen concentration field changes, and the bacterial diffusion (random swimming) and swimming velocity (directional swimming) also change. In addition, double diffusion occurs due to the difference in oxygen diffusion and bacterial diffusion (random swimming). However, it is not a double-diffusion convective problem because only bacteria contribute to the density (Metcalf & Pedley 2001). This bacterial-oxygen interaction complicates the phenomenon (Metcalf & Pedley 2001). Such interference between bacteria and oxygen affects suspension stability and bioconvective transport characteristics. In addition, when $\beta > 0$, the difference in density between water and cell causes the instability of suspension and the generation of bioconvection. However, we believe that the instability also changes depending on the difference in diffusion coefficient between cells and oxygen. In subsection 4.3, we investigate the effect of the oxygen diffusion coefficient on bioconvection.

Next, we discuss the transport phenomena of cells and oxygen in three-dimensional bioconvection at high Rayleigh number. Figure 5 shows the flow field and concentration field for $Ra = 5000$. In the cell concentration contours shown in figure 5(a), it is observed that the cells accumulating near the free surface fall toward the bottom at $x/h = 5.7$ and diffuse to the surroundings. This area of high cell concentration is a plume, and bioconvection occurs around this plume. In addition, as can be seen from figure 5(d), multiple plumes are formed in the suspension. The formation of

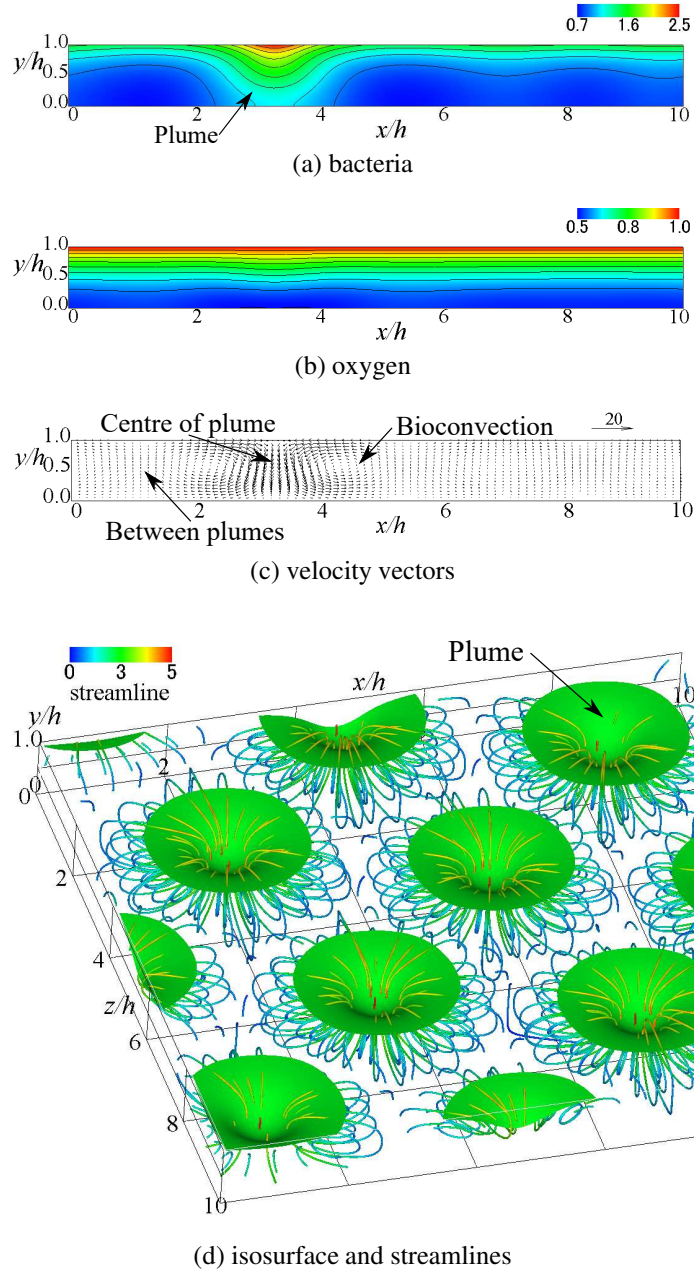


Figure 4: Bacterial and oxygen concentration contours and velocity vectors at $z/h = 6.5$, isosurface of bacterial concentration, and streamlines for $Ra = 500$: Isosurface value is 1.5.

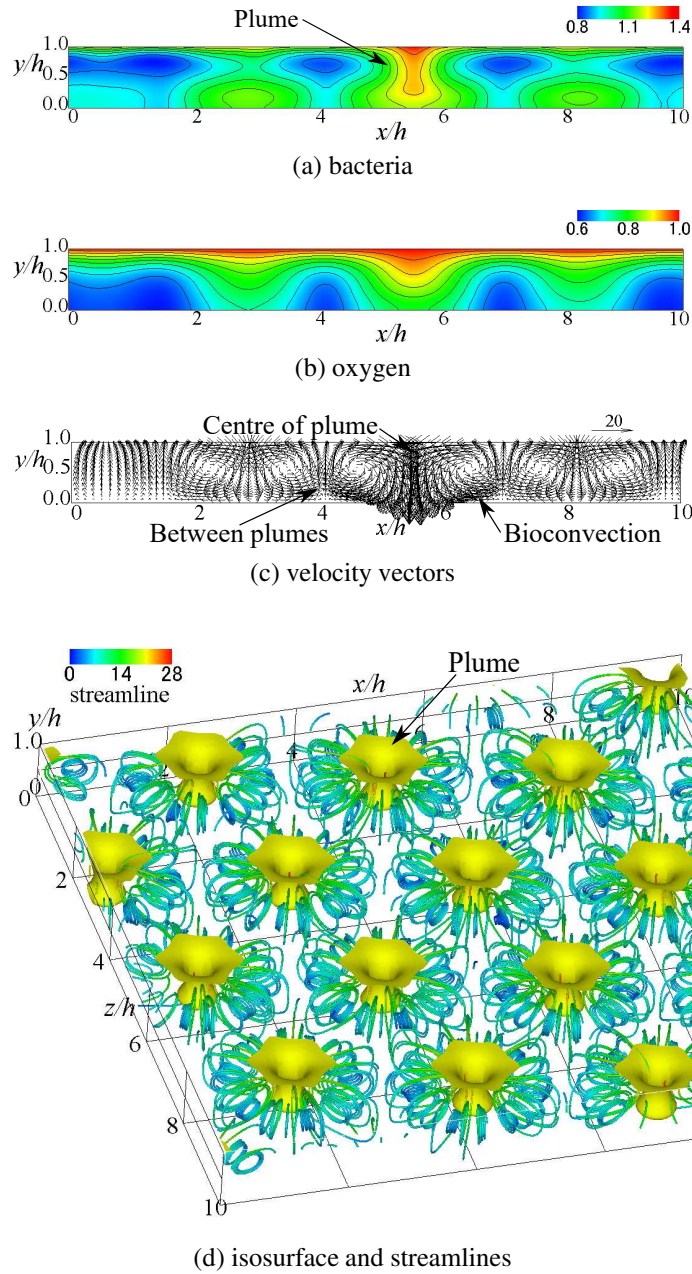


Figure 5: Bacterial and oxygen concentration contours and velocity vectors at $z/h = 4.0$, isosurface of bacterial concentration, and streamlines for $Ra = 5000$: Isosurface value is 1.2.

plumes has also been confirmed in earlier experimental studies (Bees and Hill, 1997; Jánosi et al., 1998; Czirák et al., 2000) and numerical analyses (Ghorai and Hill, 2000; Chertock et al., 2012; Karimi and Paul, 2013). Chertock et al. (2012) and Ghorai and Hill (2000) conducted two-dimensional numerical analysis, and Karimi and Paul (2013) performed three-dimensional numerical analysis. However, these works did not show the three-dimensional behavior of bioconvection. As shown in figure 5(d), this study was able to capture multiple three-dimensional plumes. In figure 5(b), more oxygen is transported toward the bottom wall in the region with the plume. This is because the bioconvection draws the fluid around the plume downward, increasing the oxygen transport due to the convection. It can be seen from figure 5(d) that the number of plumes generated in the suspension increased compared to the flow field at $Ra = 500$ and that the distance between the plumes decreased. It is found from the velocity vectors that the downward flow toward the bottom wall occurs at the centre of a plume. Inversely, it is observed that the upward flow toward the free surface occurs between the plumes and that the velocity is slower than that of the downward flow. Near the water surface, surrounding fluid concentrates toward the plume centre, so cells gather in the plume. As a result, a descending flow of high-concentration suspension occurs toward the bottom wall. Near the lower wall, the flow diffuses from the plume to the surroundings, so the ascending flow velocity between the plumes is slower than the downward flow velocity. This phenomenon can also be explained by the mathematical model used. It can be seen that if more cells are transported downward by the plume, then the downward flow velocity will increase because the downward volume force in the fundamental equation will increase. The descending and ascending flow velocities are faster than those at $Ra = 500$, and the bioconvection is stronger. It is observed from the streamlines that three-dimensional vortex rings arise around the plumes because the cells falling toward the bottom wall draw in the surrounding fluid.

For $Ra = 5000$, using the random numbers used in equation (11), we added 1% and 10% disturbances to the obtained steady-state cell concentration and continued the calculation. The converged results were the same as those before the disturbance, and the pattern of bioconvection did not change. The pattern did not change even with different initial disturbances. The suspension is stable with respect to the disturbances. Next, we perturbed the parameters related to the properties of bacteria and oxygen and investigated the effects of parameter changes on the pattern. In the present study, parameters β , γ , and δ were increased by 1%. We calculated three cases of ($\beta = 1.01$, $\gamma = \delta = 2$), ($\beta = 1$, $\gamma = 2.02$, $\delta = 2$), and ($\beta = 1$, $\gamma = 2$, $\delta = 2.02$). As a result, the pattern did not change, and there was no significant change in the flow or concentration field. From these results, we found that steady bioconvection is strongly stable with respect to disturbances.

Metcalf and Pedley (1998) investigated the patterns formed at the onset of bioconvection and clarified that the pattern is determined by the physical properties of bacteria and oxygen, such as the strength of oxygen consumption, the strength of directional swimming, and the diffusion coefficient of oxygen. Existing numerical simulations (Chertock et al. 2012; Lee & Kim 2015) have shown that changing the physical properties of bacteria and oxygen causes various bioconvection patterns. In the present study, we investigated the pattern of bioconvection by fixing these parameters and changing the Rayleigh number and initial disturbance. As will be shown later, at a high Rayleigh number, various patterns occurred when only the initial disturbance was changed. Therefore, since the stable steady-state bioconvection pattern varies depending on the initial disturbance, we can speculate that boundary conditions determine the pattern. Since the present study uses periodic boundary conditions, the initial disturbance can freely change not only the cell concentration at the boundary, but also the velocity and oxygen at the boundary, so that the bioconvection pattern can also vary. In subsection 4.8, we present calculation results for changing the chamber boundary to the side wall to investigate the effect of boundary conditions on bioconvection patterns.

4.3 Effect of physical properties of bacteria and oxygen

Theoretically, the cell and oxygen concentration distributions in a stationary fluid in a shallow chamber do not depend on the parameter δ (oxygen versus cell diffusion), but rather change only with the parameters β (oxygen consumption versus oxygen diffusion) and γ (directed versus random cell swimming) (Hillesdon and Pedley, 1996). In shallow chambers, there is enough oxygen for bacteria to be active. Hillesdon and Pedley (1996) called β (or $\beta\gamma$) depth parameters and investigated the effects of these parameters, δ and $\beta\gamma$, on the instability of suspension. As a result, when $\beta\gamma$ was changed with fixed δ , the minimum value of the critical Rayleigh number that made the suspension unstable appeared. In addition, when δ increased with fixed $\beta\gamma$, the critical Rayleigh number increased. In the present study, to clarify the effect of parameters on bioconvection, we investigate the bioconvection when the parameters δ and $\beta\gamma$ are changed under the conditions $Ra = 500$ and 5000 in which bioconvection occurs.

First, we consider the condition that the diffusion coefficient of oxygen to bacteria is large (the diffusion coefficient of bacteria is small). For $Ra = 500$, which is close to the critical Rayleigh number, δ was increased with fixed $\beta\gamma$. Figure 6 shows the oxygen concentration distribution and directional swimming velocity magnitude $V = |H(c)\gamma\nabla c|$ at $\beta = 1$, $\gamma = 2$, and $\delta = 5, 10, 20$. The theoretical value and the result of $\delta = 2$ are also shown for comparison. The cross-section is at the centre of the plume, and its position is $(x/h, z/h) = (6.6, 8.0)$ for $\delta = 5.0$, $(x/h, z/h) = (9.2, 2.6)$

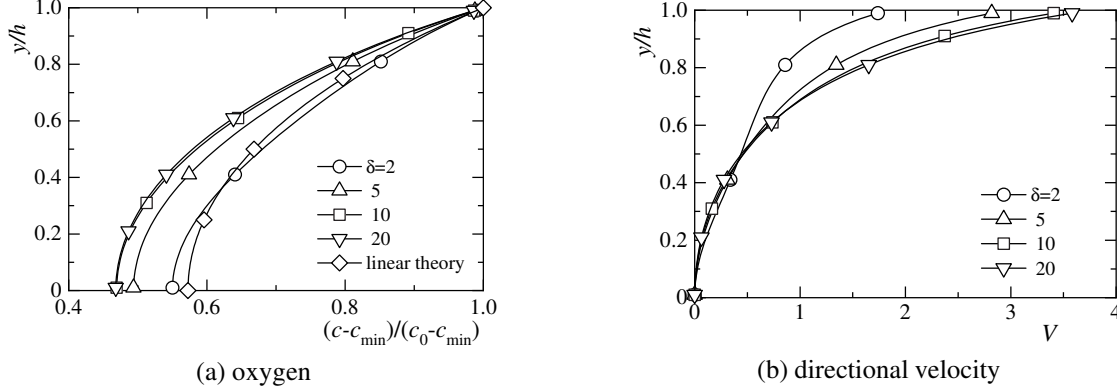


Figure 6: Distributions of oxygen concentration and directional velocity.

for $\delta = 10$, and $(x/h, z/h) = (1.7, 7.6)$ for $\delta = 20$. As δ increases, more oxygen is transported to the bottom, and the gradient of oxygen concentration in the y -direction increases, thus increasing the upward directional swimming velocity. This result leads to a decrease in cell transport due to convection (downward flow and upward directional swimming) inside plumes, which also decreases nonlinear effects. Therefore, the bioconvection decays. To compare the strength of convection, we calculated the average kinetic energy in the computational domain. The average kinetic energies are $K_{av} = 1.56, 1.03, 0.90,$ and 0.84 for $\delta = 2, 5, 10,$ and 20 , respectively, and the kinetic energy attenuates as δ increases. Although δ was increased to $\delta = 20$, the bioconvection did not disappear. The directional swimming velocity in figure 6 is the result of the plume centre. We calculated the average value V_{av} of the magnitude of the directional swimming velocity in the computational domain. For $\delta = 2, 5, 10,$ and 20 , $V_{av} = 0.542, 0.540, 0.538,$ and 0.537 , respectively. As δ increases, V_{av} decreases slightly but remains almost unchanged. This result suggests that the increase in directional swimming velocity in the plume significantly affects the attenuation of bioconvection. The numbers of plumes are 8, 5, 4, and 4 for $\delta = 2, 5, 10,$ and 20 , respectively, and the number of plumes decreases as δ increases. From the above investigation, we find that increasing δ attenuates bioconvection.

Next, we investigate the effect of bacterial-oxygen interaction on bioconvection at a high Rayleigh number. Figures 7 and 8 show the results for $\beta = 0.1$ ($\beta\gamma = 0.2$) and $\beta = 2$ ($\beta\gamma = 4$) at $\delta = 2$, respectively. In figure 8 (d), the plume is observed from below. When $\beta = 0.1$, oxygen consumption by bacteria is suppressed. Chemotactic bacteria respond to oxygen gradients and consume oxygen. When oxygen consumption decreases, bacterial activity declines because the bacteria themselves do not generate oxygen gradients. Therefore, the bioconvection at $\beta = 0.1$ is weaker than the result at $\beta = 1$ in figure 5. For $\beta = 2$, the convective velocity is higher than the result for $\beta = 1$, and more bacteria and oxygen are transported to the vicinity of the bottom surface. An increase in β means that the oxygen consumption by bacteria strengthens. As can be seen from the oxygen concentration distribution in figure 8, the oxygen consumption by bacteria increases the oxygen concentration gradient and strengthens directional swimming. At $Ra = 5000$, the upward and downward flows are strong, and if the directional swimming velocity further increases, the convection is strengthened on average in the suspension. To compare the strength of directional swimming, we calculated the average magnitude V_{av} of the directional swimming velocity in the computational domain. For $\beta = 0.1, 1,$ and 2 , $V_{av} = 6.4 \times 10^{-3}, 4.8 \times 10^{-1},$ and 1.7 , respectively, and the directional swimming velocity at $\beta = 2$ is 273 times faster than that at $\beta = 0.1$. This result shows that the bioconvection at $\beta = 0.1$ is considerably attenuated even at the high Rayleigh number. The numbers of plumes are 8, 15, and 23 for $\beta = 0.1, 1,$ and 2 , respectively, and the number of plumes increases as β increases. From the above results, we found that the rate of oxygen consumption by bacteria significantly affects the strength of bioconvection.

We investigate the enhancement of convection when directional swimming is increased without changing the rate of oxygen consumption by bacteria. Figure 9 shows the results for $\delta = 2$ and $\gamma = 10$ ($\beta\gamma = 10$). An increase in γ means an increase in the directional swimming velocity of bacteria. The bioconvection is stronger than the results for $\gamma = 2$ ($\beta\gamma = 2$) in figure 5 and $\beta = 2$ ($\beta\gamma = 4$) in figure 8. The same effect as enhancement of convection with increasing β appears. The plumes arrange randomly, and the number of plumes is 25. As the number of plumes increases, it is considered that the interference between plumes increases. The average magnitude of directional swimming velocity is $V_{av} = 9.8$, and the transport by directional swimming increases more than the results for $\beta = 0.1$ ($\beta\gamma = 0.2$), $\beta = 1$ ($\beta\gamma = 2$), and $\beta = 2$ ($\beta\gamma = 4$).

We confirmed that the bioconvection and its pattern observed in figures 7 to 9 were different from the result in figure 5. Although the Rayleigh number and initial disturbance are the same, the different bioconvections and patterns occur

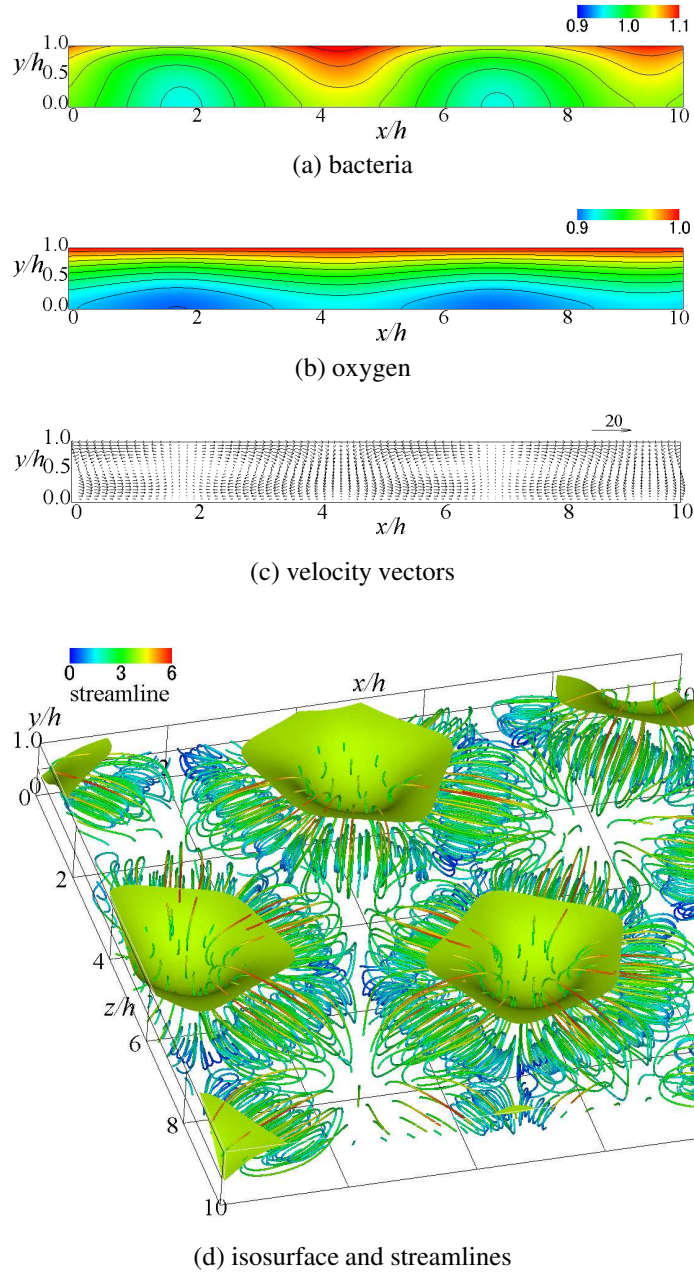


Figure 7: Bacterial and oxygen concentration contours and velocity vectors at $z/h = 0.8$, isosurface of bacterial concentration, and streamlines for $\beta = 0.1$ and $Ra = 5000$: Isosurface value is 1.06.

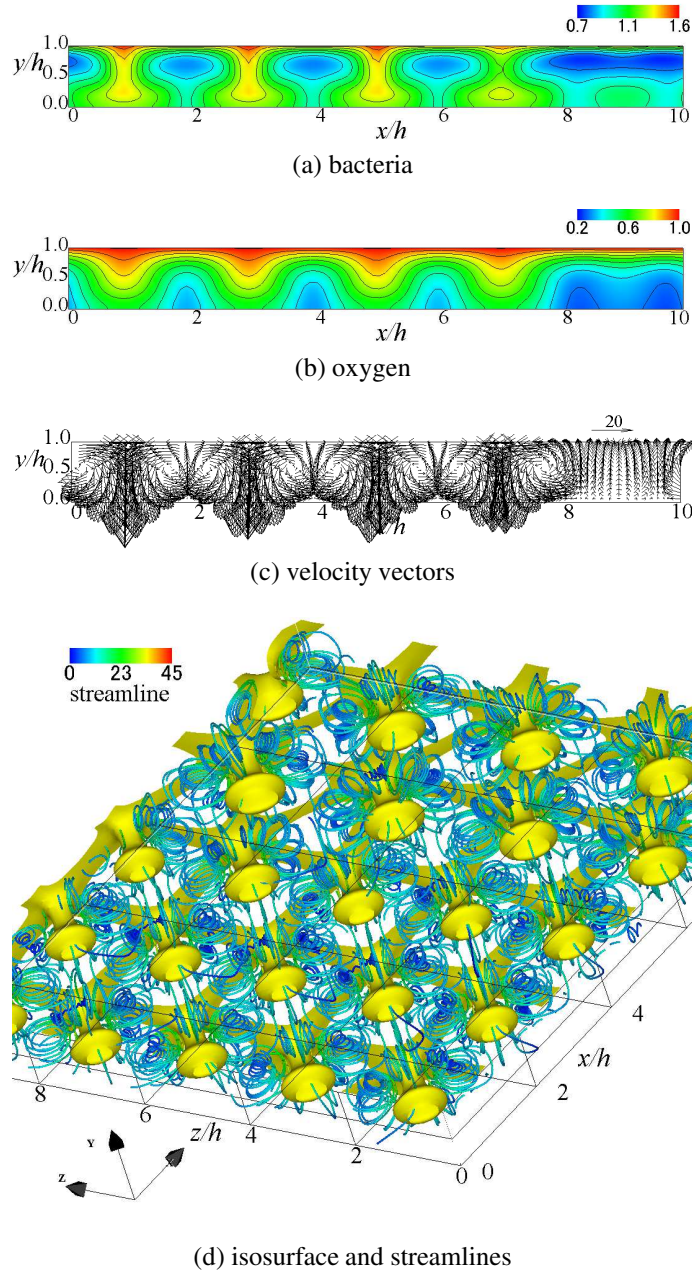


Figure 8: Bacterial and oxygen concentration contours and velocity vectors at $z/h = 1.4$, isosurface of bacterial concentration, and streamlines for $\beta = 2$ and $Ra = 5000$: Isosurface value is 1.25.

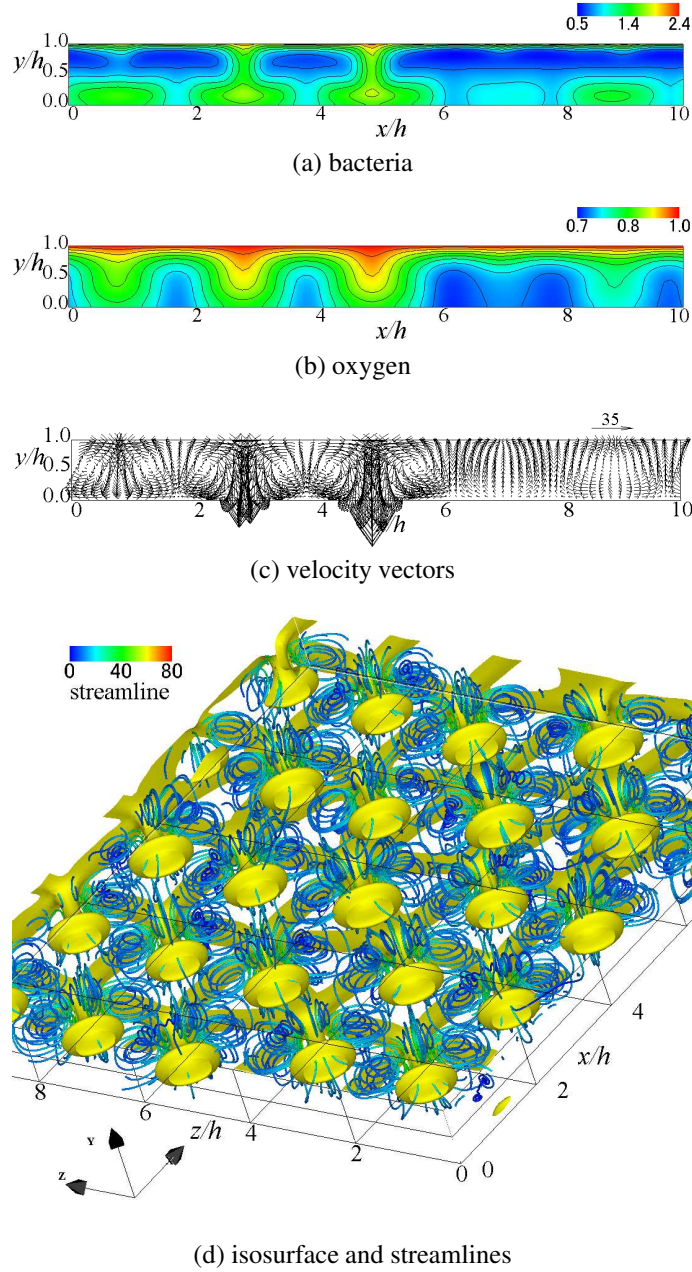


Figure 9: Bacterial and oxygen concentration contours and velocity vectors at $z/h = 4.0$, isosurface of bacterial concentration, and streamlines for $\gamma = 10$ and $Ra = 5000$: Isosurface value is 1.46.

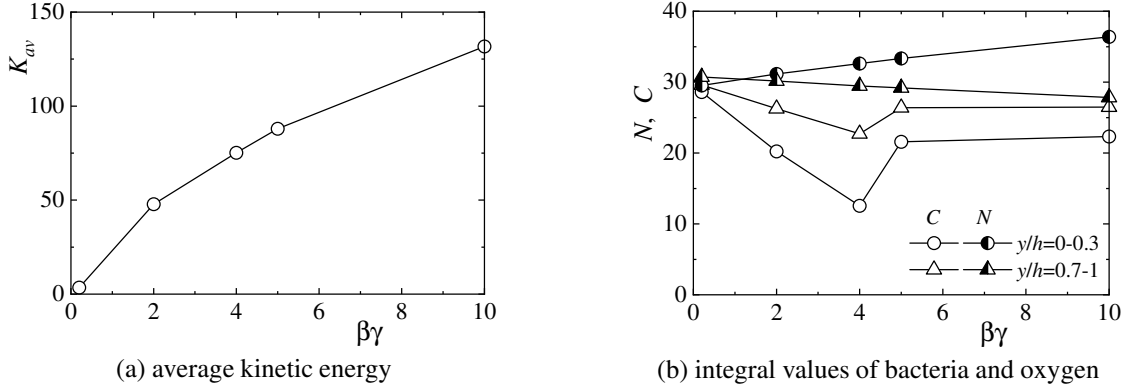


Figure 10: Average kinetic energy and integral values of bacteria and oxygen.

even if the parameters related to the physical properties of bacteria and oxygen are changed. This trend is the same as the result of the existing numerical simulations (Chertock et al., 2012; Lee and Kim, 2015).

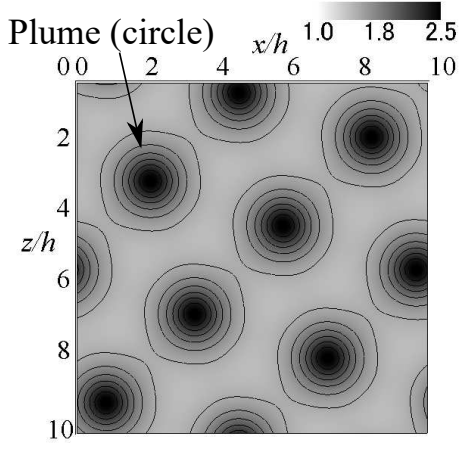
We clarify the effects of changes in the physical properties of bacteria and oxygen on the enhancement of bioconvection and the amount of transport. For $\beta = 0.1$ ($\beta\gamma = 0.2$), $\beta = 1$ ($\beta\gamma = 2$), $\beta = 2$ ($\beta\gamma = 4$), $\gamma = 5$ ($\beta\gamma = 5$), and $\gamma = 10$ ($\beta\gamma = 10$), figure 10 shows the average kinetic energy K_{av} and the integral values, N and C , of the amounts of cell and oxygen, respectively. The depth parameter $\beta\gamma$ is a parameter of the chamber depth and, at the same time, represents the parameters of the oxygen consumption rate by bacteria and the magnitude of the directional swimming velocity. In a convection-free concentration field in a shallow chamber, theoretically, the cell concentration depends only on $\beta\gamma$, while the oxygen concentration varies with $\beta\gamma$ and γ (Hillesdon and Pedley, 1996). The average kinetic energy increases with the increase of $\beta\gamma$, indicating that bioconvection strengthens. The oxygen consumption rate by bacteria or directional swimming velocity increases non-linearity and enhances convection. At this time, cell transport is improved, so many bacteria move to the vicinity of the lower wall. The cell amount decreases slightly near the water surface. Since an increase in $\beta\gamma$ increases the consumption of oxygen, the oxygen amount near the water surface and lower wall decreases. For $\beta\gamma = 5$ ($\beta = 1$, $\gamma = 5$) and $\beta\gamma = 10$ ($\beta = 1$, $\gamma = 10$), the consumption rate of oxygen by bacteria is low, so the oxygen amount does not decrease monotonically. Unlike the cell concentration, the oxygen concentration does not depend only on $\beta\gamma$, and this trend is the same as the theory (Hillesdon and Pedley, 1996).

4.4 Bioconvection pattern and wavelength of the pattern

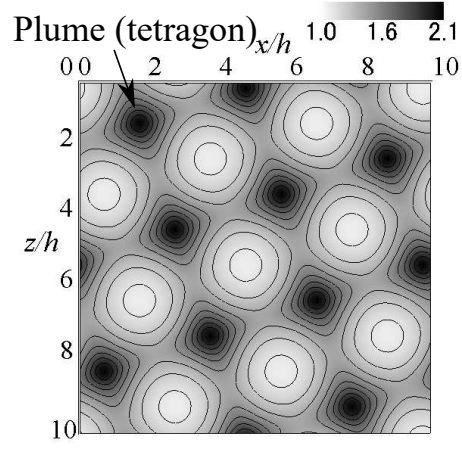
In this subsection, we discuss the influence of the initial disturbance on the bioconvection pattern and the effect of the Rayleigh number Ra on the wavelength of the pattern. Figure 11 shows cell concentration contours on the free surface for $Ra = 500, 1000, 3000$, and 5000 . The No. written with each figure corresponds to the pattern name described in table 1, with a higher contour level indicating a higher cell concentration. The plume is formed in the dark-coloured region. In figures 11(b), (c), (d), (e), and (f), the high concentration regions appear to connect adjacent plumes. Since such a pattern looks like spokes, it was called a spoke pattern in an earlier study (Mazzoni et al., 2008). Mazzoni et al. (2008) reported that the spoke patterns have been observed in previous studies on bioconvection (Platt, 1961; Jánosi et al., 1998; Czirók et al., 2000). The present study was able to confirm the spoke pattern as shown in previous studies.

Next, the arrangement of the plumes in the bioconvection patterns is compared. As shown in figures 11(a) and (d), the plumes appear in a “staggered arrangement”. The plumes in figures 11(b), (c), and (e) appear to have a “lattice arrangement”. In both the staggered and lattice arrangements, the plumes are regularly arranged. This regular plume arrangement has also been observed in a previous experiment on bioconvection (Bees and Hill, 1997) and a numerical analysis (Karimi and Paul, 2013). In contrast, since the plumes appear irregularly in figure 11(f), this pattern is defined as a “random arrangement”.

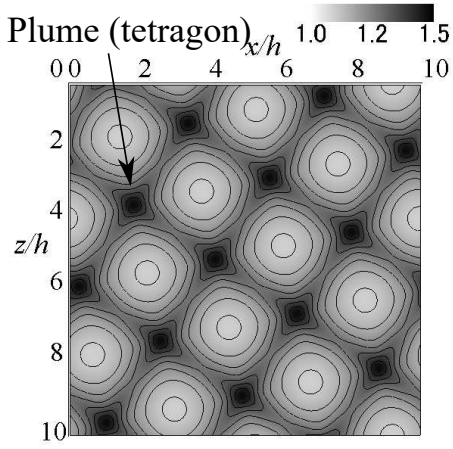
We also compare the plume shapes of each bioconvection pattern. This study defines the shape of the plumes by the number of spokes extending from one plume to the adjacent plumes in the spoke pattern. When the number of spokes extending from one plume was 4, 5, or 6, the plume shape is called a tetragon, pentagon, or hexagon, respectively. Since no spoke pattern was observed for $Ra = 500$, the plume shape is called a circle. Focusing on the relation between the arrangement and shape of the plumes, the staggered arrangement shown forms a circular or hexagonal plume, while the lattice arrangement gives rise to a tetragonal plume. As can be observed in figure 11(f), tetragonal, pentagonal, and hexagonal plumes exist in an erratic mixture in a random arrangement. Such plume shapes



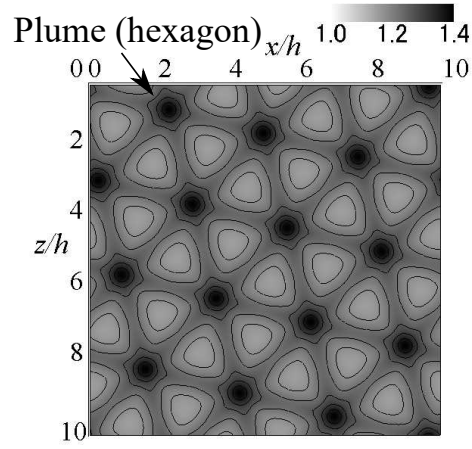
(a) No.2 ($Ra = 500$)



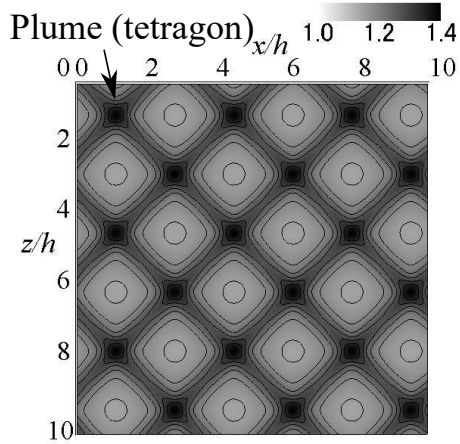
(b) No.11 ($Ra = 1000$)



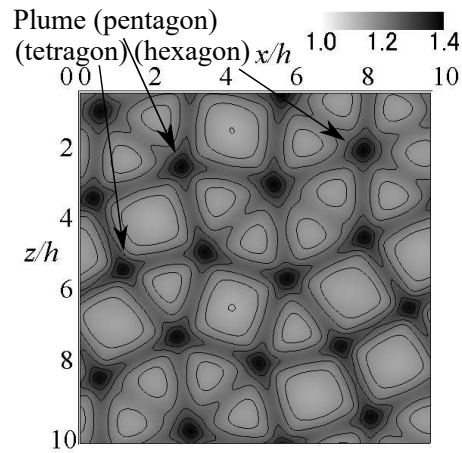
(c) No.13 ($Ra = 3000$)



(d) No.16 ($Ra = 5000$)



(e) No.17 ($Ra = 5000$)



(f) No.21 ($Ra = 5000$)

Figure 11: Bacterial concentration contours in x - z plane at $y/h = 1.0$ for $Ra = 500, 1000, 3000, 5000$.

pattern's name	Ra	arrangement	shape	λ/h	pattern's name	Ra	arrangement	shape	λ/h
No.1	500	staggered	circle	3.54	No.13	3000	lattice	tetragon	2.77
No.2	500	staggered	circle	3.54	No.14	4000	lattice	tetragon	2.50
No.3	500	staggered	circle	3.54	No.15	5000	random	mixture	2.50
No.4	500	staggered	circle	3.54	No.16	5000	staggered	hexagon	2.43
No.5	500	staggered	circle	3.54	No.17	5000	lattice	tetragon	2.36
No.6	500	random	circle	3.54	No.18	5000	random	mixture	2.24
No.7	500	staggered	circle	3.54	No.19	5000	random	mixture	2.24
No.8	500	lattice	tetragon	3.33	No.20	5000	random	mixture	2.43
No.9	500	staggered	circle	3.16	No.21	5000	random	mixture	2.24
No.10	500	random	circle	3.54	No.22	5000	lattice	tetragon	2.43
No.11	1000	lattice	tetragon	3.16	No.23	5000	lattice	tetragon	2.43
No.12	2000	staggered	tetragon	2.77	No.24	5000	random	mixture	2.50

Table 1: Rayleigh number Ra , arrangement of plumes, shape of plumes and pattern wavelength λ/h .

have been confirmed in a previous experiment and numerical studies on bioconvection. The experimental result by [Bees and Hill \(1997\)](#) indicated that tetragonal or hexagonal plumes regularly form arrays in a long-term pattern. This result corresponds to the tetragonal and hexagonal plumes observed in this study. The experiment of [Czirók et al. \(2000\)](#) showed that hexagonal plumes occur at the final pattern mode of bioconvection. A numerical analysis by [Karimi and Paul \(2013\)](#) confirmed the formation of a star-shaped plume. As can be seen by observing this plume in detail, a region of high cell concentration extends from one plume to an adjacent plume in five directions. This star-shaped plume is similar to the pentagonal plume defined in this study.

Table 1 shows the plume arrangement, plume shape, and wavelength λ/h of the bioconvection pattern for each Rayleigh number. Here, the wavelength of the pattern was calculated using a two-dimensional fast Fourier transform of the cell concentration on the free surface as in previous studies ([Bees and Hill, 1997](#); [Czirók et al., 2000](#); [Williams and Bees, 2011](#); [Kage et al., 2013](#)). First, we investigate the influence of the given initial disturbance in the cell concentration on the bioconvection patterns. This study used the initial cell concentration with ten different disturbances for $Ra = 500$ and 5000. At $Ra = 500$, the circular plumes showed a staggered arrangement for many of the calculation conditions, and no significant changes in the bioconvection pattern due to the initial disturbance were observed. In contrast, for $Ra = 5000$, various bioconvection patterns including the staggered, lattice, and random arrangements occur due to the initial disturbances. This result indicates that even for the same Rayleigh number, bioconvection patterns with different plume arrangements, shapes, and numbers can arise due to the effects of different kinds of initial disturbances and that the wavelengths of the bioconvection patterns are different. In a previous experiment ([Bees and Hill, 1997](#)), it was reported that it is difficult to achieve a homogeneous cell concentration as the ideal initial state of the suspension because fluid motion after mixing the suspension remains. [Bees and Hill \(1997\)](#) found that the wavelengths of the bioconvection patterns also varied, accompanying the pattern change, even though the same cell concentration and suspension depth were set. In this study, initial disturbances are added to the initial conditions of the cell concentration to simulate the initial state in the previous experiment ([Bees and Hill, 1997](#)). From this result, it can be concluded that the present study confirms the phenomenon observed in the previous study. As mentioned above, it is found that more significant changes in the bioconvection pattern due to the initial disturbance appears at high Rayleigh number because the increase in the Rayleigh number enhances the non-linearity. Finally, comparing the wavelengths of the patterns in table 1, it is confirmed that the wavelengths of the bioconvection patterns are changed depending on the plume arrangement. In addition, the wavelength of the pattern becomes shorter as the Rayleigh number increases.

4.5 Wavelength comparison with previous results

Next, we compare this numerical result with previous results for the wavelengths of bioconvection patterns. [Bees and Hill \(1997\)](#) conducted experiments on bioconvection formed by single-celled alga *Chlamydomonas nivalis* and investigated the wavelengths of the bioconvection patterns at the onset of bioconvection and in a long-term pattern. They found that the wavelength decreases with increasing cell concentration and that the cell concentration has a significant effect on the wavelength of the pattern. [Czirók et al. \(2000\)](#) experimentally investigated the bioconvection formed by *Bacillus subtilis* and measured the wavelength of the bioconvection pattern at the onset of bioconvection. They clarified that the wavelength decreases with increasing in cell concentration measured by optical density measurements. To compare our numerical results with earlier experimental results using the Rayleigh number, we calculated the Rayleigh number of the experimental data. The volume of a cell V , density ratio of a cell to water $(\rho_n - \rho)/\rho$, water kinematic viscosity ν , and cell diffusivity D_{n0} were not described in Bees and Hill's paper, so we used values

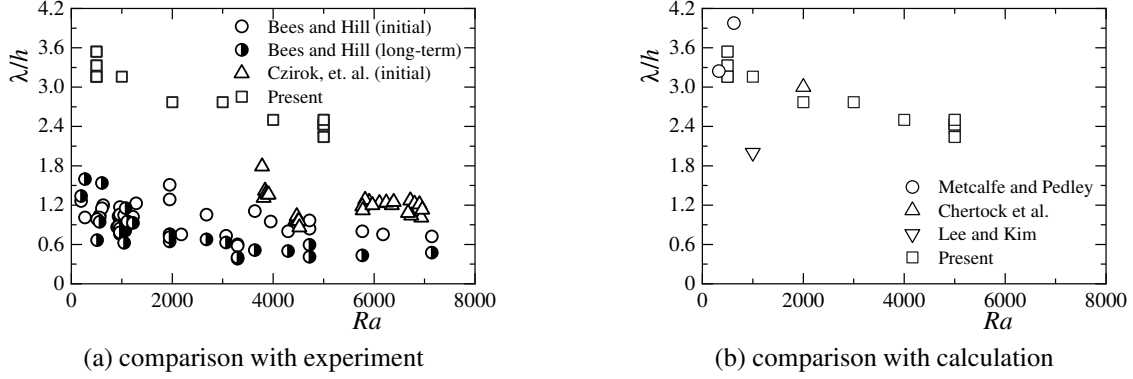


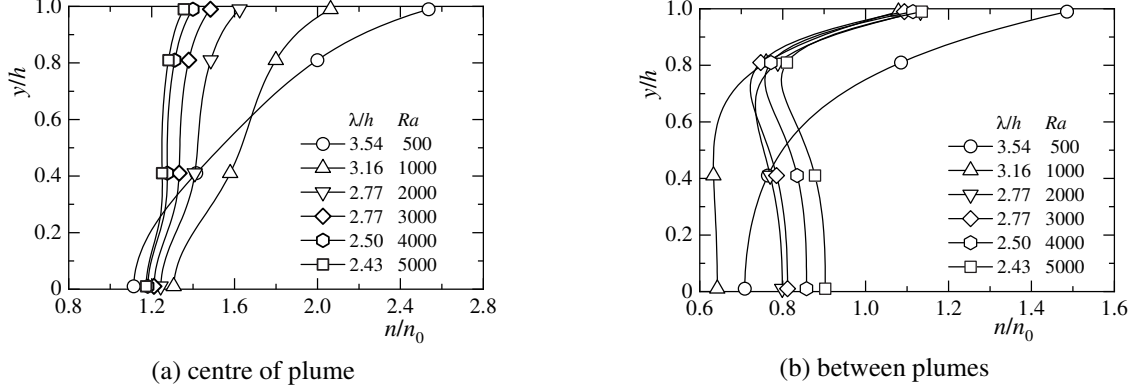
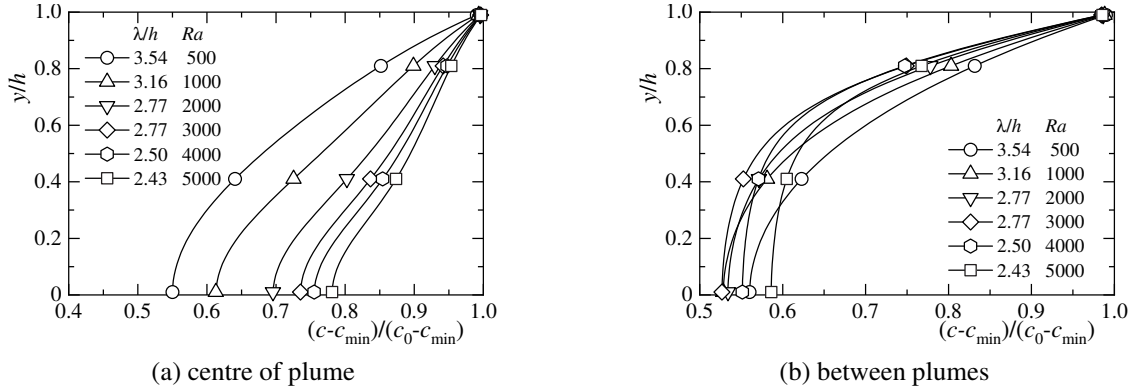
Figure 12: Comparison of pattern wavelength with previous results (Bees and Hill, 1997; Czirik et al., 2000; Metcalfe and Pedley, 1998; Chertock et al., 2012; Lee and Kim, 2015).

from Ghorai and Hill (2002). Likewise, V , $(\rho_n - \rho)/\rho$, ν , and D_{n0} were not mentioned in Czirik et al. (2000), so we took ν from Hillesdon and Pedley (1996), and other values from János et al. (1998). The gravity acceleration g was not reported in these papers (Hillesdon and Pedley, 1996; Bees and Hill, 1997; János et al., 1998; Czirik et al., 2000; Ghorai and Hill, 2002), and thus we took g from Pedley et al. (1988). The numerator of the Rayleigh number equation (10) defined in this paper includes the initial cell concentration n_0 . Thus, it can be considered that increasing the Rayleigh number increases the initial cell concentration.

Figure 12 shows a comparison between our numerical values and experimental values (Bees and Hill, 1997; Czirik et al., 2000) for the bioconvection pattern. The trend of the wavelength of the pattern to decrease with increasing Rayleigh number is qualitatively consistent with the experimental results. However, there is a quantitative difference between the wavelengths in this calculation and the experiments.

Metcalfe and Pedley (1998) used weakly nonlinear analysis to determine the critical wavenumber and critical Rayleigh number at which a suspension becomes unstable. We obtained the wavelength at the critical Rayleigh number for two conditions ($\gamma\beta = 1$, $\delta = 1$, $Sc = 7700$) and ($\gamma\beta = 50$, $\delta = 1$, $Sc = 7700$) in the existing research. In addition, using the previous calculations (Chertock et al., 2012; Lee and Kim, 2015), we calculate the wavelength of the bioconvection pattern generated when an initial disturbance is given by random numbers. The parameters in the calculation of Chertock et al. (2012) are $\beta = 4$, $\gamma = 10$, $\delta = 5$, and $Sc = 500$, and the parameters in the calculation of Lee and Kim (2015) are $\beta = 2$, $\gamma = 10$, $\delta = 5$, and $Sc = 500$. We calculated the wavelength from the number of plumes and the length of the calculation area. Figure 12 (b) compares the wavelength derived from the previous results with the present results. In all analyses using chemotactic bacteria, the parameters used are different, but the previous results are in the range of $\lambda/h = 2.0 - 4.0$. These values are overestimated as compared to the experimental values for all Rayleigh numbers. Thus, further investigations into this difference are required.

Earlier studies (Bees and Hill, 1997; Ghorai and Hill, 2002; Williams and Bees, 2011) reported similarities between bioconvection and thermal convection. Therefore, the patterns observed in previous experiments for thermal convection (Koschmieder and Switzer, 1992) and in numerical analysis (Tomita and Abe, 2000) and the wavelengths of the patterns are compared with the present values. Koschmieder and Switzer (1992) showed that the number of convection cells increased as the temperature difference applied to the fluid increased. In that paper, the Rayleigh number is defined, and an increase in temperature difference corresponds to an increase in the Rayleigh number. An increase in the number of convection cells means a decrease in the spacing between convection cells, that is, the wavelength of the pattern. Tomita and Abe (2000) investigated Bénard–Marangoni convection and found that the wavelength of the pattern decreases as the parameter that combines the Rayleigh and Marangoni numbers increases. Increasing this parameter means increasing the Rayleigh number. Therefore, it can be said that the trend of the wavelength of the bioconvection pattern to decrease with increasing Rayleigh number is qualitatively consistent with the result of thermal convection. Furthermore, when comparing the patterns, the hexagonal convection pattern observed in the previous studies (Koschmieder and Switzer, 1992; Tomita and Abe, 2000) is similar to the hexagonal-shaped plume observed in the present study. The wavelength of the hexagonal convection pattern (Tomita and Abe, 2000) is $2.71 \leq \lambda/h \leq 2.94$, which is similar to the wavelength of the bioconvection pattern observed in this study.


 Figure 13: Bacterial concentration distributions in y -direction at plume centre and between plumes.

 Figure 14: Oxygen concentration distributions in y -direction at plume centre and between plumes.

4.6 Interference between plumes

We discuss the influence of the wavelength variation of the bioconvection pattern on the concentration field. First, figures 13 and 14 show the distribution of cell and oxygen concentrations in the y -direction at the plume centre and between plumes. Here, No.2 ($Ra = 500$), No.11 ($Ra = 1000$), No.12 ($Ra = 2000$), No.13 ($Ra = 3000$), No.14 ($Ra = 4000$), and No.16 ($Ra = 5000$) in table 1 are used for the results. All these results used the same initial disturbance. We consider the positions at the plume centre and between the plumes as being the points where the cell concentrations on the free surface become maximum and minimum, respectively. The positions of the plume centres at $Ra = 500, 1000, 2000, 3000, 4000, 5000$ are $(x/h, z/h) = (4.7, 0.4), (5.8, 3.2), (8.0, 0.5), (1.9, 3.5), (1.5, 8.8), (2.3, 0.8)$, and the positions between the plumes are $(x/h, z/h) = (3.4, 1.6), (5.8, 8.2), (3.0, 6.2), (6.9, 8.5), (7.7, 2.6), (6.1, 2.6)$.

In the centre of the plume, as the wavelength of the pattern decreases, the amount of the cell transported by the downward flow increases, so the cell concentration near the water surface decreases. As can be seen from figures 4 and 5, bioconvection strengthens as the wavelength of the pattern decreases, and the plume extending to the lower wall diffuses to the surroundings. This indicates that the cell amount transported from the plume centre to between the plumes increases. Therefore, as the wavelength decreases, the cell concentration near the lower wall decreases at the plume centre, converges to a constant value, and increases between the plumes. The cell concentration near the water surface between the plumes does not change depending on the wavelength, except at $Ra = 500$, and is lower than the concentration at the plume centre. At $Ra = 500$, the bioconvection is weak, so the trend is different from the results at other Rayleigh numbers.

Next, we consider the oxygen concentration. At the plume centre, the oxygen concentration near the lower wall increases because the oxygen transported by the downward flow increases as the wavelength of the pattern decreases. Between the plumes, the oxygen concentration decreases at $\lambda/h > 2.77$ ($Ra < 3000$) as the wavelength decreases. This is because as the wavelength decreases, the amount of cells transported between plumes increases and the amount of oxygen consumed increases. On the other hand, the tendency of $\lambda/h \leq 2.77$ ($Ra \geq 3000$) is different from the result of $\lambda/h > 2.77$ ($Ra < 3000$), and the oxygen concentration increases as the wavelength decreases. This

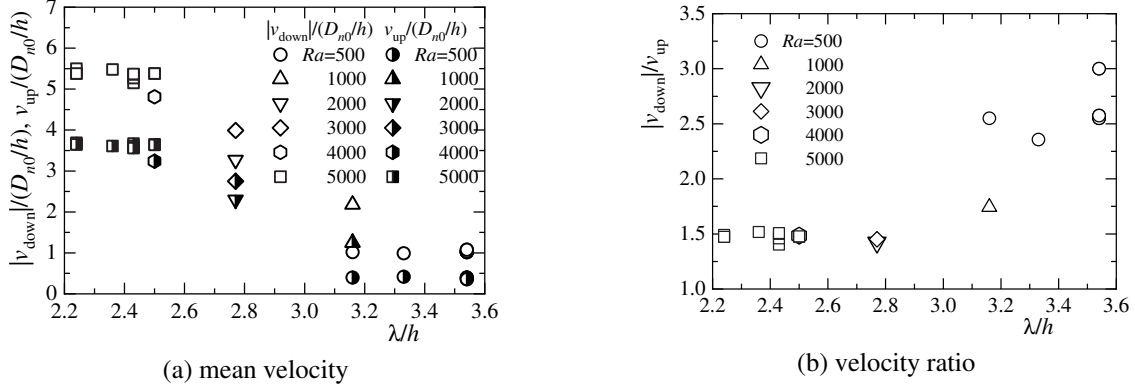


Figure 15: Mean velocities of downward and upward flows.

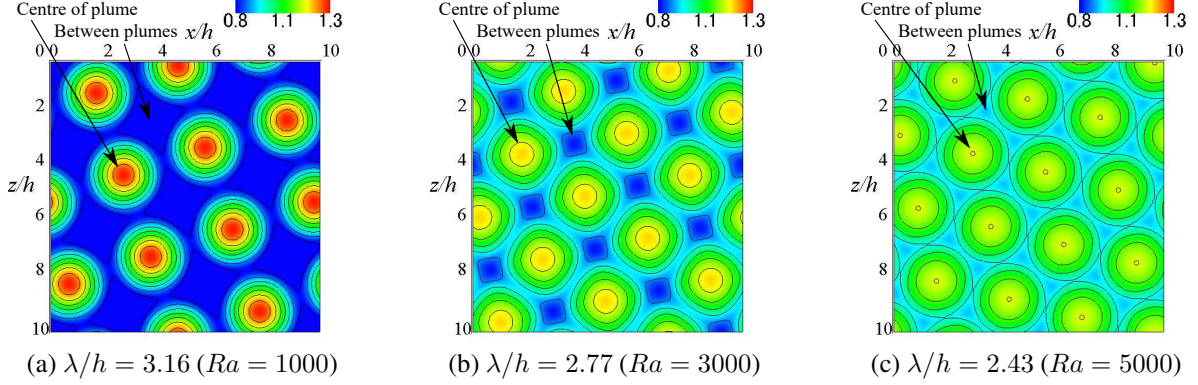
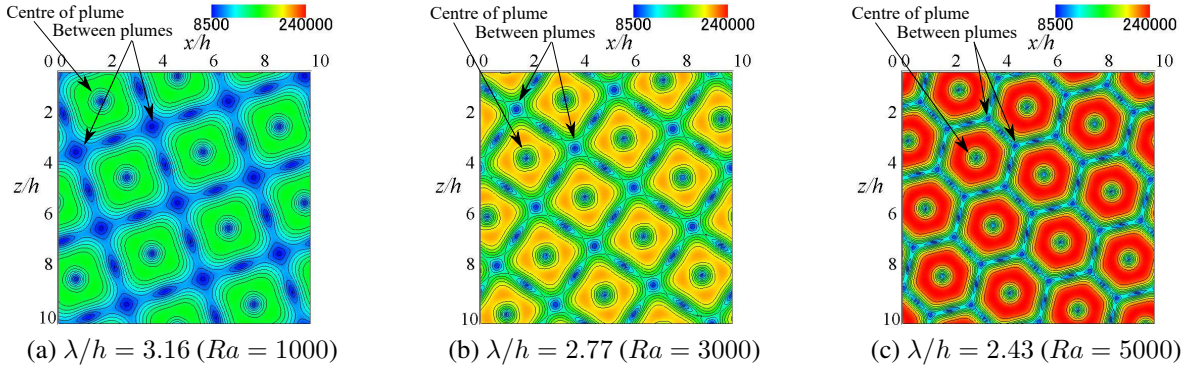
is because, as the wavelength decreases, bioconvection strengthens and the amount of oxygen transported between plumes exceeds the amount of oxygen consumed by bacteria.

This study calculated the mean velocity, v_{down} , of the downward flow at the centre of the plume, and the mean velocity, v_{up} , of the upward flow between plumes. v_{down} and v_{up} are defined by averaging the vertical velocities such that $v < 0$ and $v > 0$, respectively. Figure 15 (a) shows the relationship between the wavelength of the pattern and mean velocities, v_{down} and v_{up} . In the figure, the wavelength of the pattern decreases as the Rayleigh number increases, and then $|v_{\text{down}}|$ increases at the centre of the plume. Also, we can observe the same tendency in v_{up} between the plumes shown in the figure. This result occurs because the interference between plumes has increased. In other words, as the wavelength of the pattern becomes shorter, the plumes approach each other, and the velocities of the downward flow and the upward flow increase. In addition, we have observed in figure 5 that the velocity of the downward flow is faster than that of the upward flow. The wavelengths of the patterns for $Ra = 2000$ and $Ra = 3000$ have the same values. However, as can be seen from $|v_{\text{down}}|$ and v_{up} , the flow velocities of $Ra = 3000$ are faster than those of $Ra = 2000$. This result is because the number of cells transported downward increases as the Rayleigh number increases, and then the bioconvection is strengthened.

Figure 15 (b) shows the ratio of the downward velocity to the upward velocity. This ratio is also related to the volume occupied by the plumes and the volume occupied between the plumes. As can be seen in figure 5, the plumes with high cell concentrations are narrower than the areas between the plumes. Figure 15 (b) shows that if the net upward and downward transports are balanced on average, then the velocity of the descending flow in the plume will be faster than that of the upward flow, and the area occupied by the plume will become small. When the wavelength is large, the velocity ratio reaches three, and the area of influence of the downward flow in the plume on the cell transport becomes narrow. As the wavelength decreases, the velocity ratio decreases. This suggests that the ascending flow velocity increases and the area of influence of the ascending flow on the cell transport becomes narrow.

To compare the strength of convection in each pattern, the average kinetic energy within the calculation domain was calculated for $Ra = 5000$. If the kinetic energy is high, it can be said that the convection is strong on average. The mean value obtained from the average kinetic energy of all patterns was $K_{av} = 47.2$, and the standard deviation was 0.341. We find that the strength of bioconvection does not depend on the pattern.

We investigate the influence of the shear flow near the wall surface on bacteria. The surface friction coefficient C_f on the bottom wall is defined as $C_f = \tau_w / [\rho(D_{n0}/h)^2/2]$, where $\tau_w = \mu(\partial V/\partial y)$, and V is a composite component of the velocities in the x - and z -directions. Figures 16 and 17 show the contours of the cell concentration at $y/h = 0.01$ and the surface friction coefficient using the data of No.11 ($Ra = 1000$), No.13 ($Ra = 3000$), and No.16 ($Ra = 5000$) in table 1. The same initial disturbance is applied to all these results. In the region where the plumes exist, the cell concentration becomes high, and it can be seen that a large amount of bacteria exists under the plumes. Comparing the results for each Rayleigh number, we observe that the cell concentration decreases in the centre of a plume and increases between the plumes as the wavelength of the bioconvection pattern decreases. It is found that the surface friction coefficient is large in the region of a plume and that a strong shear flow occurs in this region. Also, the wall friction coefficient increases as the wavelength of the pattern decreases. Therefore, the cells under the plumes are affected by strong shear stress. Van der Pol and Tramper (1998) investigated the influence of shear stress on animal cells and reported that shear stress causes damage to animal cells and cell death. In future research, it will be interesting to investigate the influence of shear stress on bacteria due to bioconvection.


 Figure 16: Bacterial concentration contours in x - z plane at $y/h = 0.01$ for $Ra = 1000, 3000, 5000$.

 Figure 17: Surface friction coefficient contours in x - z plane at the lower wall for $Ra = 1000, 3000, 5000$.

4.7 Transport characteristics

To clarify the transport characteristics of cells and oxygen, we investigated the variations of each flux distribution. As in previous studies (Yanaoka et al., 2007, 2008), the flux of cells and oxygen is defined as

$$J_n^{\text{total}} = J_n^{\text{conv}} + J_n^{\text{diff}} + J_n^{\text{swim}} \quad (12)$$

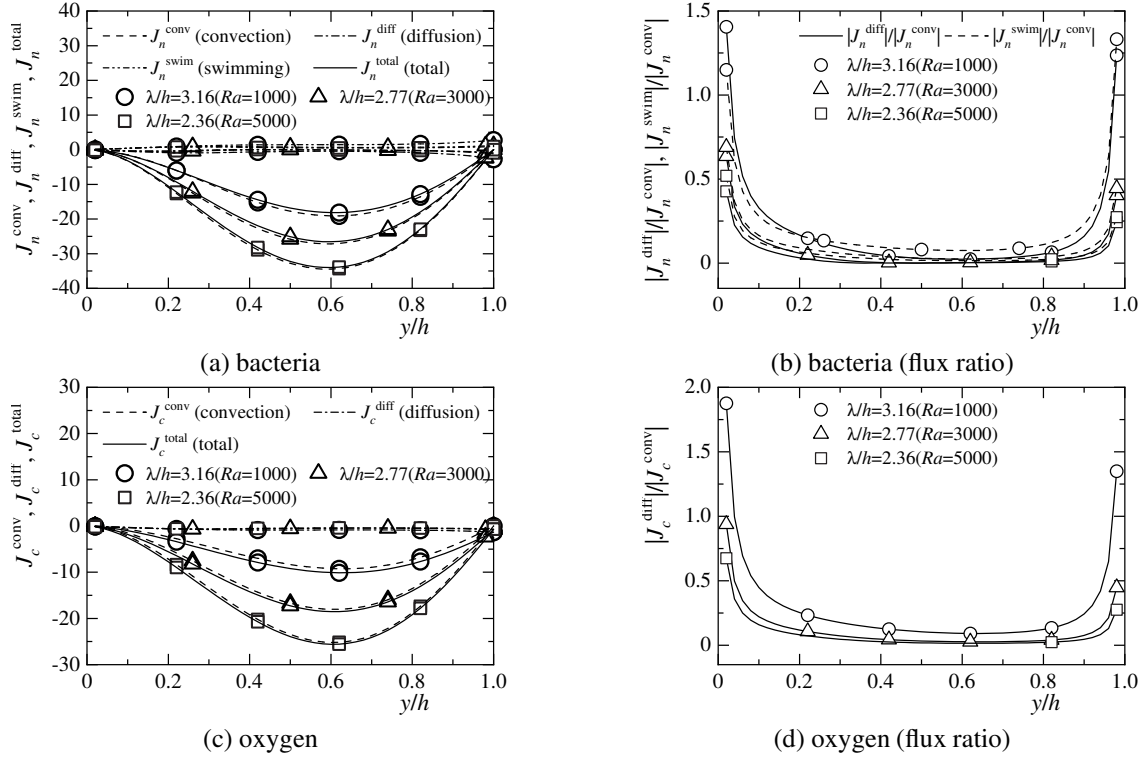
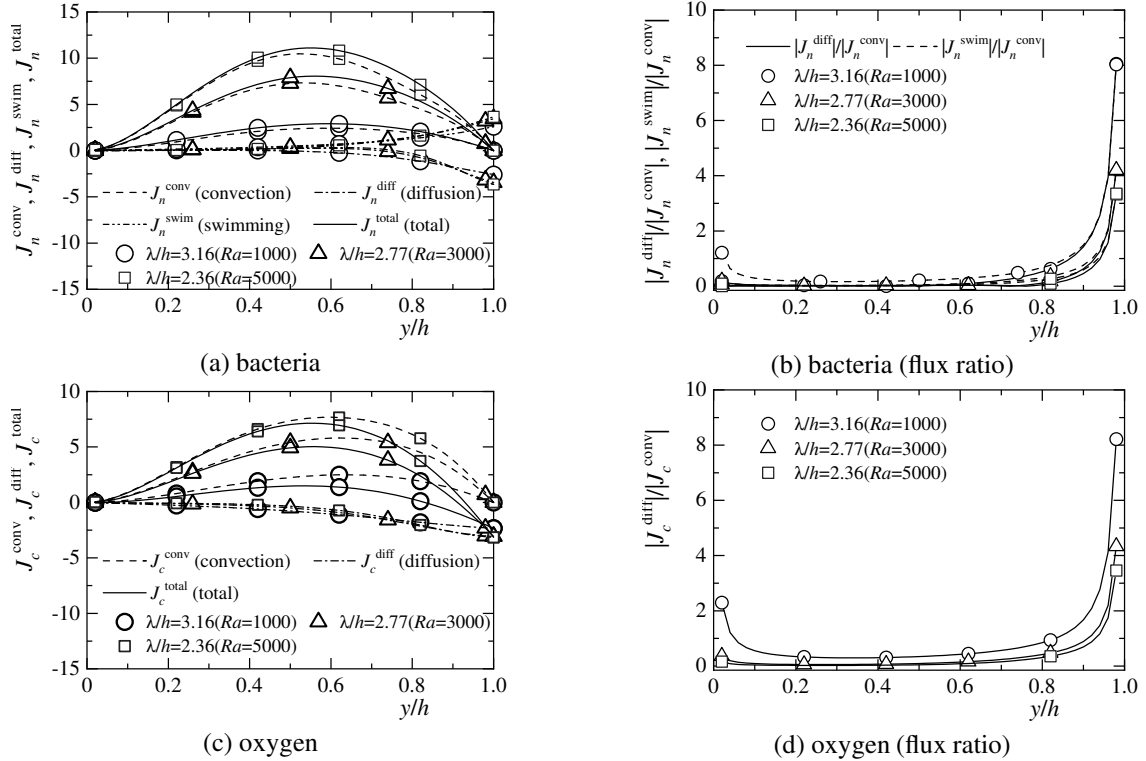
$$J_c^{\text{total}} = J_c^{\text{conv}} + J_c^{\text{diff}} \quad (13)$$

where J_n^{total} is the total flux of cells, J_c^{total} is the total flux of oxygen, J_n^{conv} is the convective flux of cells, J_c^{conv} is the convective flux of oxygen, J_n^{diff} is the diffusive flux of cells, J_c^{diff} is the diffusive flux of oxygen, and J_n^{swim} is the swimming flux of cells. These fluxes are given as

$$J_n^{\text{conv}} = \mathbf{u}n, \quad J_n^{\text{diff}} = -H(c)\nabla n, \quad J_n^{\text{swim}} = H(c)\gamma n \nabla c \quad (14)$$

$$J_c^{\text{conv}} = \mathbf{u}c, \quad J_c^{\text{diff}} = -\delta \nabla c \quad (15)$$

For $Ra = 1000, 3000,$ and 5000 , figures 18 and 19 show the cell and oxygen flux distributions in the y -direction at the centre of a plume and between the plumes, respectively. The results shown are for a lattice arrangement (figures 11(b), (c), and (e)) in which plumes are regularly arrayed. For $Ra = 1000, 3000,$ and 5000 , the positions of the plume centres are $(x/h, z/h) = (5.8, 3.2), (1.9, 3.5),$ and $(6.2, 6.0)$, and the positions between the plumes are $(x/h, z/h) = (5.8, 8.2), (6.9, 8.5),$ and $(1.2, 6.0)$. At the centre of a plume, the cell and oxygen transport due to the convection are dominant throughout the region. In the velocity vectors shown in figure 5, the convective velocity increased near $y/h = 0.6$, where the flows around the plume joined together. Thus, the transport by the convection becomes active there. These trends are similar between the plumes, but because the convective velocity between the plumes is slower, the convective transport between the plumes becomes smaller than that at the centre of a plume. The flux ratios are also shown in figures 18 and 19. The previous study (Chertock et al., 2012) also discussed transport characteristics using the flux ratio. Near the lower wall and the water surface in the centre of the plume, the cell transport by random swimming (diffusion) and directional swimming and the oxygen transport by diffusion increase compared to


 Figure 18: Flux distributions of bacteria and oxygen in y -direction at the centre of a plume.

 Figure 19: Flux distributions of bacteria and oxygen in y -direction between plumes.

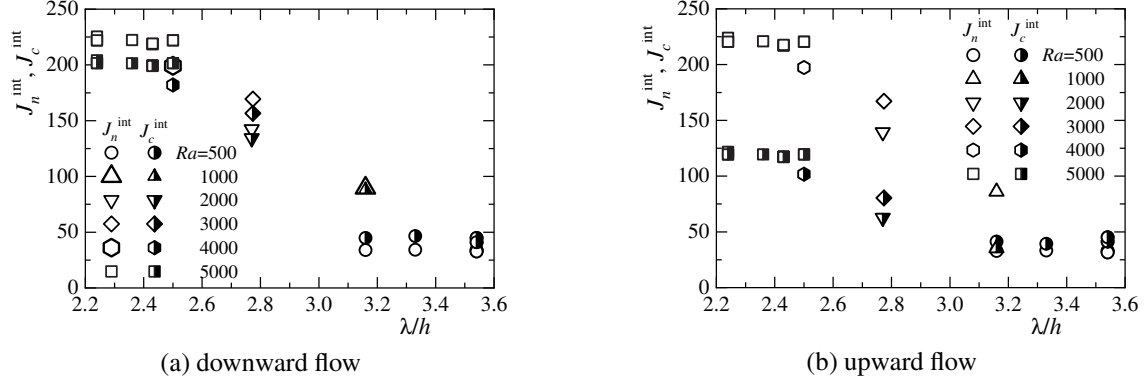
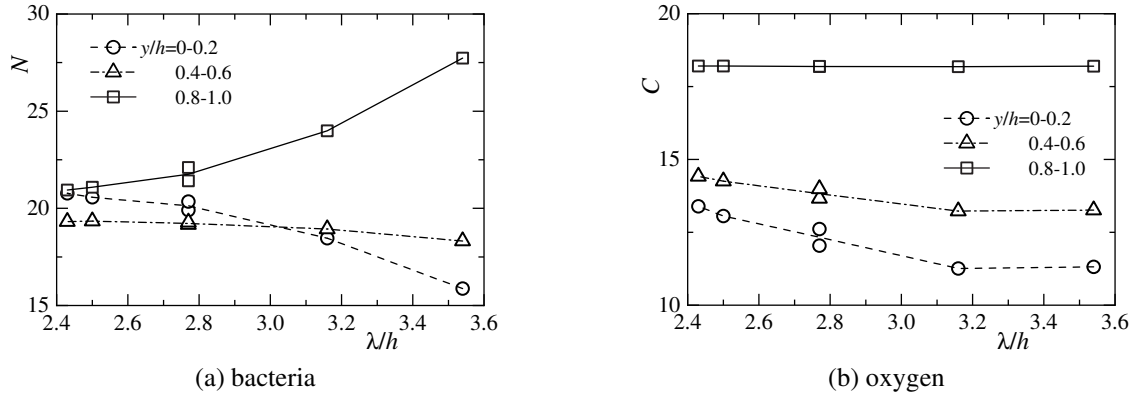

 Figure 20: Integral values of total flux of bacteria and oxygen in y -direction for downward flow and upward flow.


Figure 21: Integral values of bacterial and oxygen concentrations.

the transport by convection. At small wavelengths, the transport by directional swimming is slightly larger than the transport by random swimming. In contrast, the cell transport by diffusion and swimming is large near the free surface between the plumes, and the cells are actively moving. Here, the cell transport due to the directional and random swimming is almost in balance. Since the oxygen is supplied from the free surface of the suspension by diffusion, the oxygen transport increases toward the free surface. The flux ratios indicate that the transport by swimming and diffusion between the plumes is relatively larger than the transport by convection, as compared to the centre of the plume, because the convective transport by the upward flow is smaller than that by the downward flow.

Next, we compare the transport characteristics of cells and oxygen for each wavelength of the bioconvection pattern. The total flux of cells and oxygen increase with decreasing wavelength at plume centres and between the plumes. The reason is as follows. As the wavelength decrease enhances interference between plumes, increasing the downward and upward flow velocities at the plume centre and between the plumes. Therefore, the transport of cells and oxygen by convection increases. As can be seen from the flux ratios, the cell transport due to diffusion and swimming is low regardless of wavelength, except near the bottom wall and the water surface. Near the water surface between plumes, the flux ratios vary significantly with the wavelength. As the wavelength decreases, the cell transport by diffusion and swimming and the oxygen transport by diffusion decrease compared to the convective transport.

To clarify the influence of the wavelength of the pattern on the transport characteristics over the entire suspension, the integral values of the total flux of cells and oxygen, J_n^{int} and J_c^{int} , were evaluated. These values are obtained by integrating $|J_n^{\text{total}}|$ and $|J_c^{\text{total}}|$ over the entire suspension. We consider the transport characteristics of cells and oxygen for the downward and upward flows. Figure 20 shows the relationship between J_n^{int} and J_c^{int} of the total flux of cells and oxygen and the wavelength λ/h of the pattern. As the Rayleigh number increases, the wavelength decreases and interference between the plumes increases, which improves the transport characteristics of the cells and oxygen due to the downward flow. These trends are similar in the upward flow region. From the above, it can be said that because the transport characteristics due to the downward and upward flows improve with decreasing wavelength, the transport characteristics over the entire suspension also improve.

To investigate the effects of pattern wavelength changes on the transport of bacteria and oxygen, we calculate the integral values, N and C , of the amounts of cells and oxygen, respectively, near the bottom wall ($0 \leq y/h \leq 0.2$), in the middle ($0.4 \leq y/h \leq 0.6$), and near the water surface ($0.8 \leq y/h \leq 1.0$). Here, the results of No. 2 ($Ra = 500$), No. 11 ($Ra = 1000$), No. 12 ($Ra = 2000$), No. 13 ($Ra = 3000$), No. 14 ($Ra = 4000$), and No. 16 ($Ra = 5000$) in table 1 are shown in figure 21. These are the results when the same initial disturbance is given. As the wavelength decreases, the cell amount decreases near the water surface and increases near the bottom wall. This is because the transport characteristics improve as the wavelength decreases, and the cell amount that settles downward increases. At $\lambda/h = 3.54$, the difference between the cell amounts near the bottom wall and near the water surface is large, but the difference decreases as the wavelength decreases. The cell amount near the middle increases slightly as the wavelength decreases, but at $\lambda/h < 3.16$, the cell amount becomes approximately constant. The oxygen amount increases near the bottom wall and in the middle area because the oxygen transport characteristics improve as the wavelength decreases. The oxygen amount near the water surface is approximately constant. Since the bacteria that gather downward consume oxygen, the oxygen amount decreases toward the depth at each wavelength. It was found from the above results that the amounts of cells and oxygen near the bottom wall increase because the transport characteristics improve as the pattern wavelength decreases.

4.8 Influences of computational region and boundary condition

To confirm that the above results do not depend on the calculation region, we compare the results for the computational regions of $L = 10h$ and $20h$ for $Ra = 5000$. The same initial disturbance for $L = 10h$ in figure 5 was set for $L = 20h$. Figure 22 shows the flow field and concentration field at $L = 20h$. As in figure 5, it can be seen that bioconvection with multiple plumes occurs. In the bioconvection pattern in figure 22(d), a lattice arrangement in the region of $x/h \geq 10$, a staggered arrangement in $5 \leq x/h \leq 10$, $z/h \geq 10$, and random arrangements in $x/h \leq 10$, $0 \leq z/h \leq 10$ appear. It is found from this result that the bioconvection patterns observed at $L = 10h$ appear simultaneously. The wavelength of the bioconvection pattern for $L = 20h$ is $\lambda/h = 2.34$. We calculated the averaged wavelength for $L = 10h$ to compare the results of $L = 10h$ and $20h$. The wavelength was $\lambda/h = 2.38$, which was obtained by averaging the wavelengths of all patterns for $L = 10h$. The difference between the wavelength for $L = 10h$ and $L = 20h$ is approximately 1.71%, and it can be said that the wavelengths of the bioconvection patterns observed at $L = 10h$ and $20h$ are almost the same. As with $L = 10h$, it is possible that bioconvection patterns with different wavelengths will occur for different initial disturbances.

Next, we investigate the transport characteristics of the cells and oxygen over the entire suspension for $L = 20h$. The integral values of the total flux are $J_n^{\text{int}} = 1767.2$ and $J_c^{\text{int}} = 1297.9$. To compare the results of $L = 10h$ and $20h$, we averaged the integrated value of the total flux of each pattern for $L = 10h$, and the values were $J_n^{\text{int}} = 440.8$ and $J_c^{\text{int}} = 323.8$. To compare these values with the result for $L = 20h$, which is 4 times the computational region of $L = 10h$, J_n^{int} and J_c^{int} for $L = 10h$ are multiplied by 4, and the difference between the results for $L = 10h$ and $L = 20h$ is found to be approximately 0.23% and 0.21%, respectively. The results for $L = 10h$ and $20h$ are almost the same. Comparing the calculation results for $L = 10h$ and $L = 20h$, the same results were obtained for the wavelength and transport characteristics of the bioconvection pattern, even for different computational regions. Therefore, it can be seen that the results for $L = 10h$ do not depend on the computational region.

The pattern of Rayleigh-Bénard convection changes depending on the system geometry and boundary conditions (Cross and Hohenberg, 1993; Bodenschatz et al., 2000). Similarly, it is considered that the pattern of bioconvection changes. Metcalfe and Pedley (1998) mentioned that the side wall of the Petri dish affects the pattern. Yamamoto et al. (1992) also clarified that the vessel's wall determines the pattern generation. Figure 23 shows the calculation result for changing the chamber boundary to side walls. In this calculation, the calculation conditions are the same as those using periodic boundary conditions, and the given initial disturbance is also the same. Plumes line up along the boundaries. A pattern with more regularity than the result in figure 22 occurs. Bacteria adhere to all side walls, and plumes form near the walls. Therefore, downward flow occurs near all side walls. The same regular pattern as in figure 23 was obtained even with different initial disturbances. Since bacteria gather near the water surface before bioconvection occurs, bacteria adhere to the side wall. Subsequently, the suspension becomes unstable, and plumes form. Since the velocity is slow near the wall due to the non-slip condition, the bacteria adhered to the side wall are less likely to come off, and even if bioconvection develops, the bacteria may remain attached to the side wall. The integrated values of the total flux are $J_n^{\text{int}} = 1789.5$ and $J_c^{\text{int}} = 1326.0$, and the differences from the results when using the periodic boundary condition are 1.3 – 2.2%. Therefore, there is no difference in transport characteristics due to the boundary conditions. Karimi and Paul (2013) performed a numerical analysis on gyrotactic bioconvection and reported that the pattern at the final stage does not depend on boundary conditions. This trend differs from our calculation results. Since the present result is a converged solution after sufficient time has passed, it is considered that this regular pattern does not collapse. Karimi and Paul (2013) reported that the final pattern did not reach a steady state, so this discrepancy with the existing result may be due to the difference between steady state and transient state but requires further investigation.

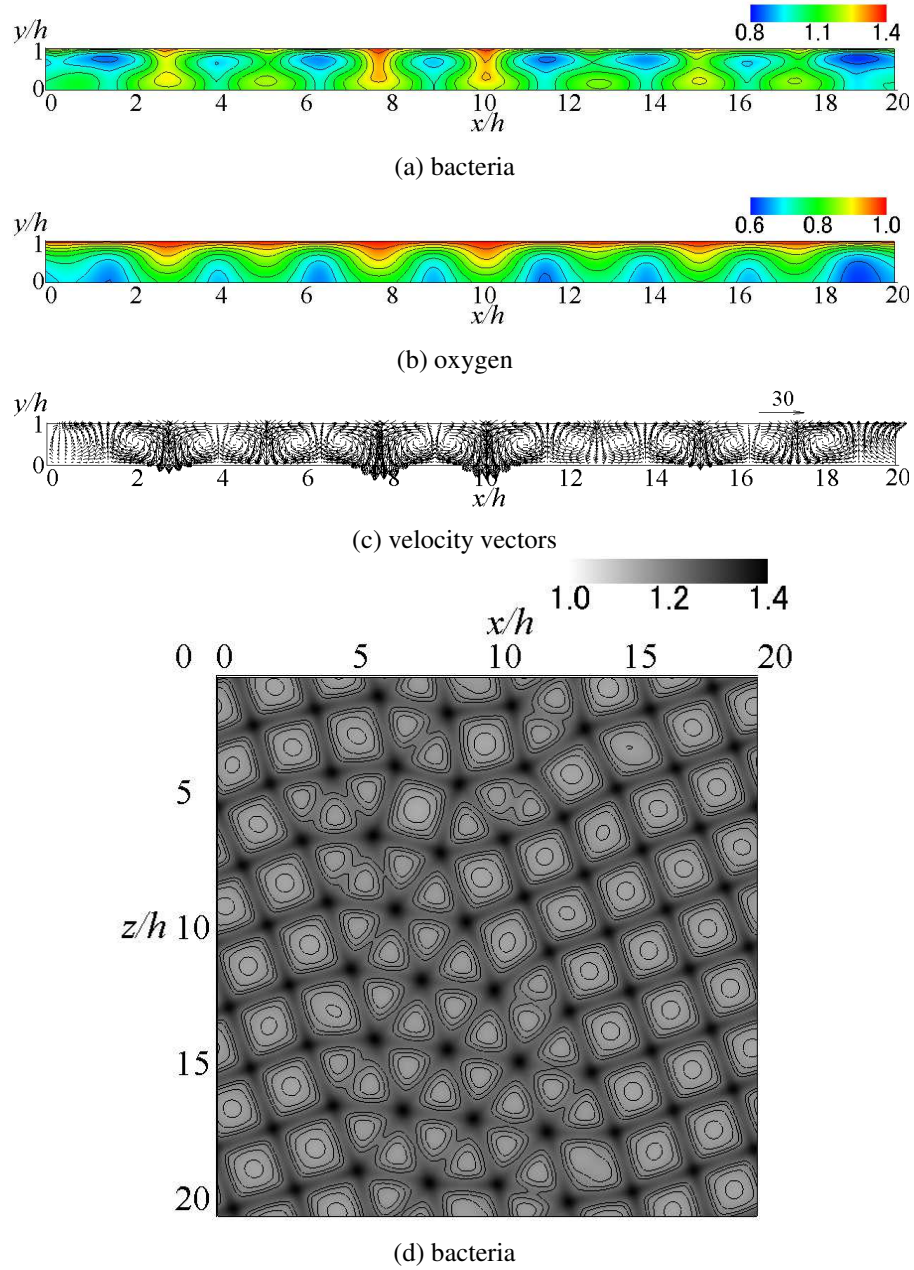


Figure 22: Bacterial and oxygen concentration contours, velocity vectors at $z/h = 18.8$, and bacterial concentration contours at $y/h = 1.0$ for $Ra = 5000$.

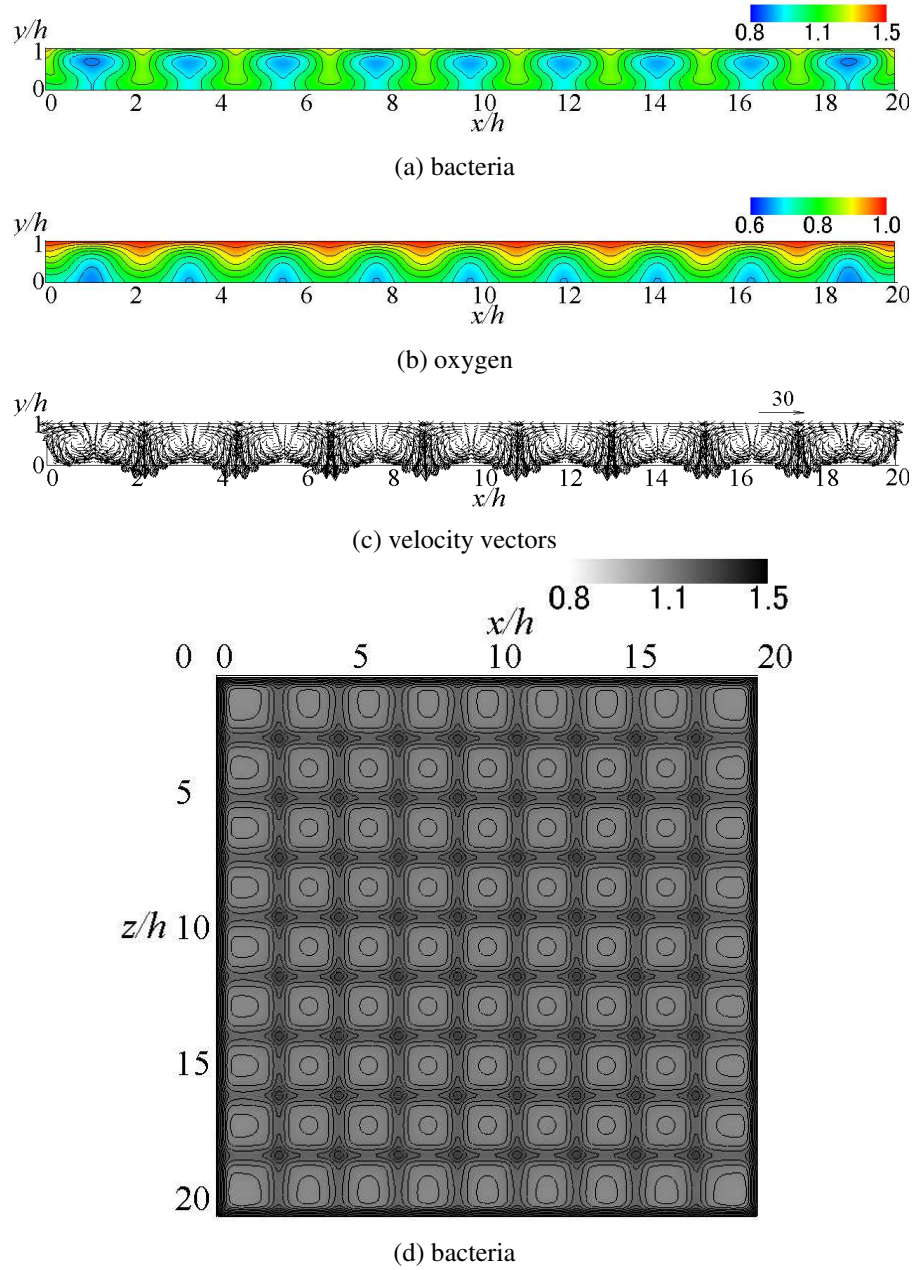


Figure 23: Bacterial and oxygen concentration contours, velocity vectors at $z/h = 8.9$, and bacterial concentration contours at $y/h = 1.0$ for $Ra = 5000$ in chamber with side walls.

When using the periodic boundary condition, changing the initial disturbance can change not only the cell concentration on the boundary, but also the velocity and oxygen, so that the bioconvection pattern can also vary. If the side wall is set, bacteria will adhere to the wall surface. Therefore, it is considered that the pattern is difficult to change freely. Since we impose a condition of zero cell flux at the side wall, bacterial adhesion is a natural consequence. However, it is still necessary to investigate the cause of bacteria remaining attached to the side wall. In bioconvection, in which plumes interact with each other, the adhesion phenomenon of bacteria to walls has not been investigated in detail. Therefore, such investigations will be the subject of future research.

5 Conclusions

We conducted a three-dimensional numerical simulation on bioconvection generated by oxygen-reactive chemotactic bacteria. The bioconvection patterns, interference between plumes, wavelength of the bioconvection pattern, and transport characteristics of cells and oxygen were investigated when multiple plumes occurred in the suspension. The findings obtained are summarized as follows.

- (1) When the Rayleigh number reaches the critical value, multiple three-dimensional plumes arise in the suspension. Three-dimensional bioconvection occurs around the plumes and vortex rings form around the plumes. Even if bioconvection at a high Rayleigh number is disturbed, the bioconvection is strongly stable with respect to disturbances, and the pattern does not change due to disturbances.
- (2) The ratio of the diffusion coefficient of oxygen to bacteria greatly affects the strength of bioconvection, and when the diffusion coefficient of oxygen is relatively large, bioconvection becomes weak. The rate of oxygen consumption by bacteria significantly affects the strength of bioconvection, and the stronger the oxygen consumption by bacteria, the stronger the bioconvection. This trend to strengthen bioconvection is also the same when the directional swimming velocity of bacteria increases.
- (3) Bioconvection patterns with different plume arrangements and shapes are formed for different Rayleigh numbers or initial disturbances of the cell concentration. Thus, the wavelengths of the patterns also vary. Comparing the arrangement and shape of the plumes, a staggered arrangement is observed consisting of circular or hexagonal plumes, a lattice arrangement constituted by tetragonal plumes, and a random arrangement consisting of plumes with various shapes.
- (4) As the Rayleigh number increases, interference between the plumes is strengthened by the decrease in wavelength of the pattern. Thus, the velocities of both the upward and downward flows increase. The velocity of the downward flow is faster than that of the upward flow.
- (5) Many cells are located under plumes, and a strong shear flow occurs in these regions. As the wavelength of the pattern decreases, the shear stress increases. Therefore, many cells are affected by a strong shear stress.
- (6) The convective transport of the entire suspension strengthens as the wavelength of the pattern decreases. Therefore, the transport characteristics of cells and oxygen improve, and then the amounts of cells and oxygen transported near the bottom wall in the suspension increases.
- (7) When the chamber boundary is changed to side walls, bacteria adhere to the wall surface, and plumes are regularly arranged along the side walls. Periodic boundary conditions can cause various patterns of bioconvection, while the side wall may suppress free formations of patterns.

In the present study, we investigated the effect of the chamber side wall on the pattern of bioconvection and found that the side wall changed the pattern. This time, we used a rectangular container with side walls. The chamber geometry may change the pattern of bioconvection and accompanying transport characteristics, so that further investigation of bioconvection under different boundary conditions is necessary. In addition, since characteristics such as the oxygen consumption rate of bacteria significantly affect bioconvection, advanced mathematical models are required. More detailed experimental information will be useful for developing mathematical models, and it is thought that the investigation of transport characteristics by numerical analysis will develop. Furthermore, it is necessary to investigate the control of bioconvection for the engineering application of bioconvection. We have investigated the interference between bioconvection and thermal convection by heating suspension and the improvement of transport characteristics, and we plan to report the results in the future.

Acknowledgments. The numerical results in this research were obtained using the supercomputing resources at Cyberscience Center, Tohoku University. We would like to express our gratitude to Associate Professor Yosuke

Suenaga of Iwate University for his support of my laboratory. The authors wish to acknowledge the time and effort of everyone involved in this study.

Funding. This work was supported by Grants-in-Aid for Scientific Research C from Japan Society for the Promotion of Science (grant number 24560181).

Declaration of Interests. The authors report no conflict of interest.

Author ORCID.

Yanaoka H. <https://orcid.org/0000-0002-4875-8174>.

Author contributions. H. Yanaoka conceived and planned the research and developed the calculation method and numerical codes. T. Nishimura performed the simulations. All authors contributed equally to analysing data and reaching conclusions, and in writing the paper.

References

- Amsden, A.A., Harlow, F.H., 1970. A simplified MAC technique for incompressible fluid flow calculations. *J. Comput. Phys.* 6, 322–325. doi:doi:[https://doi.org/10.1016/0021-9991\(70\)90029-X](https://doi.org/10.1016/0021-9991(70)90029-X).
- Bees, M.A., Croze, O.A., 2014. Mathematics for streamlined biofuel production from unicellular algae. *Biofuels* 5, 53–65. doi:doi:<https://doi.org/10.4155/bfs.13.66>.
- Bees, M.A., Hill, N.A., 1997. Wavelengths of bioconvection patterns. *J. Exp. Biol.* 200, 1515–1526. doi:doi:<https://doi.org/10.1242/jeb.200.10.1515>.
- Berg, H.C., Brown, D.A., 1972. Chemotaxis in *escherichia coli* analysed by three-dimensional tracking. *Nature* 239, 500–504. doi:doi:<https://doi.org/10.1038/239500a0>.
- Bodenschatz, E., Pesch, W., Ahlers, G., 2000. Recent developments in rayleigh-bénard convection. *Annu. Rev. Fluid Mech.* 32, 709–778. doi:doi:<https://doi.org/10.1146/annurev.fluid.32.1.709>.
- Chertock, A., Fellner, K., Kurganov, A., Lorz, A., Markowich, P.A., 2012. Sinking, merging and stationary plumes in a coupled chemotaxis–fluid model: A high-resolution numerical approach. *J. Fluid Mech.* 694, 155–190. doi:doi:<https://doi.org/10.1017/jfm.2011.534>.
- Cross, M.C., Hohenberg, P.C., 1993. Pattern formation outside of equilibrium. *Rev. Mod. Phys.* 65, 851–1112. doi:doi:<https://doi.org/10.1103/RevModPhys.65.851>.
- Czirók, A., Jánosi, I.M., Kessler, J.O., 2000. Bioconvective dynamics : dependence on organism behaviour. *J. Exp. Biol.* 203, 3345–3354. doi:doi:<https://doi.org/10.1242/jeb.203.21.3345>.
- Geng, P., Kuznetsov, A.V., 2005. Settling of bidispersed small solid particles in a dilute suspension containing gyrotactic micro-organisms. *Int J Eng Sci* 43, 992–1010. doi:doi:<https://doi.org/10.1016/j.jengsci.2005.03.002>.
- Ghorai, S., Hill, N.A., 2000. Wavelengths of gyrotactic plumes in bioconvection. *Bull. Math. Biol.* 62, 429–450. doi:doi:<https://doi.org/10.1006/bulm.1999.0160>.
- Ghorai, S., Hill, N.A., 2002. Axisymmetric bioconvection in a cylinder. *J. Theor. Biol.* 219, 137–152. doi:doi:<https://doi.org/10.1006/jtbi.2002.3077>.
- Hart, A., Edwards, C., 1987. Buoyant density fluctuations during the cell cycle of *bacillus subtilis*. *Arch. Microbiol.* 147, 68–72. doi:doi:<https://doi.org/10.1007/BF00492907>.
- Hillesdon, A.J., Pedley, T.J., 1996. Bioconvection in suspensions of oxytactic bacteria: Linear theory. *J. Fluid Mech.* 324, 223–259. doi:doi:<https://doi.org/10.1017/S0022112096007902>.
- Hillesdon, A.J., Pedley, T.J., Kessler, J.O., 1995. The development of concentration gradients in a suspension of chemotactic bacteria. *Bull. Math. Biol.* 57, 299–344. doi:doi:<https://doi.org/10.1007/BF02460620>.
- Hirooka, T., Nagase, H., 2003. Biodegradation of endocrine disrupting chemicals and its application for bioremediation –utilization of photoautotrophic microorganisms–. *J. Environ. Biotechnol.* 3, 23–32. (in Japanese).
- Itoh, A., Toida, H., Saotome, Y., 2001. Control of bioconvection and its application for mechanical system (1st report, basic effects of electrical field on bioconvection). *JSME, Ser. B* 67, 2449–2454. doi:doi:<https://doi.org/10.1299/kikaib.67.2449>. (in Japanese).

- Itoh, A., Toida, H., Saotome, Y., 2006. Control of bioconvection and its application for mechanical system (2nd report, pitch optimization of electrodes array and driving of mechanical system by controlled bioconvection). JSME, Ser. B 72, 972–978. doi:doi:<https://doi.org/10.1299/kikaib.72.972>. (in Japanese).
- Jánosi, I.M., Kessler, J.O., Horváth, V.K., 1998. Onset of bioconvection in suspensions of *bacillus subtilis*. Phys. Rev. E 58, 4793–4800. doi:doi:<https://link.aps.org/doi/10.1103/PhysRevE.58.4793>.
- Kage, A., Hosoya, C., Baba, S.A., Mogami, Y., 2013. Drastic reorganization of bioconvection pattern of *chlamydomonas*: Quantitative analysis of the pattern transition response. J. Exp. Biol. 216, 4557–4566. doi:doi:<https://doi.org/10.1242/jeb.092791>.
- Karimi, A., Paul, M.R., 2013. Bioconvection in spatially extended domains. Phys. Rev. E 87, 053016. doi:doi:<https://link.aps.org/doi/10.1103/PhysRevE.87.053016>.
- Khan, M., Salahuddin, T., Malik, M.Y., Alqarni, M.S., Alqahtani, A.M., 2020. Numerical modeling and analysis of bioconvection on MHD flow due to an upper paraboloid surface of revolution. Physica A 553, 124231. doi:doi:<https://doi.org/10.1016/j.physa.2020.124231>.
- Koschmieder, E.L., Switzer, D.W., 1992. The wavenumbers of supercritical surface-tension-driven Bénard convection. J. Fluid Mech. 240, 533–548. doi:doi:<https://doi.org/10.1017/S0022112092000181>.
- Kuznetsov, A.V., 2005. The onset of bioconvection in a suspension of negatively geotactic microorganisms with highfrequency vertical vibration. Int. Commun. Heat Mass Transf. 32, 1119–1127. doi:doi:<https://doi.org/10.1016/j.icheatmasstransfer.2005.05.004>.
- Kuznetsov, A.V., 2011. Nanofluid bioconvection: interaction of microorganisms oxytactic upswimming, nanoparticle distribution, and heating/cooling from below. Theor. Comput. Fluid Dyn. 26, 291–310. doi:doi:<https://doi.org/10.1007/s00162-011-0230-1>.
- Lee, H.G., Kim, J., 2015. Numerical investigation of falling bacterial plumes caused by bioconvection in a three-dimensional chamber. Eur. J. Mech. B Fluids 52, 120–130. doi:doi:<https://doi.org/10.1016/j.euromechflu.2015.03.002>.
- Matsumoto, M., Nishimura, T., 1998. Mersenne twister: A 623-dimensionally equidistributed uniform pseudo-random number generator. ACM Trans. Model. Comput. Simul. 8, 3–30. doi:doi:<https://doi.org/10.1145/272991.272995>.
- Mazzoni, S., Giavazzi, F., Cerbino, R., Giglio, M., Vailati, A., 2008. Mutual voronoi tessellation in spoke pattern convection. Phys. Rev. Lett. 100, 188104. doi:doi:<https://link.aps.org/doi/10.1103/PhysRevLett.100.188104>.
- Metcalf, A.M., Pedley, T.J., 1998. Bacterial bioconvection: Weakly nonlinear theory for pattern selection. J. Fluid Mech. 370, 249–270. doi:doi:<https://doi.org/10.1017/s0022112098001979>.
- Metcalf, A.M., Pedley, T.J., 2001. Falling plumes in bacterial bioconvection. J. Fluid Mech. 445, 121–149. doi:doi:<https://doi.org/10.1017/s0022112001005547>.
- Naseem, F., Shafiq, A., Zhao, L., Naseem, A., 2017. MHD biconvective flow of Powell Eyring nanofluid over stretched surface. AIP Adv. 7, 065013. doi:doi:<https://doi.org/10.1063/1.4983014>.
- Noever, D.A., Matsos, H.C., 1991a. A bioassay for monitoring cadmium based on bioconvective patterns. J. Environ. Sci. Health A 26, 273–286. doi:doi:<https://doi.org/10.1080/10934529109375633>.
- Noever, D.A., Matsos, H.C., 1991b. Calcium protection from cadmium poisoning: Bioconvective indicators in *tetrahymena*. J. Environ. Sci. Health A 26, 1105–1113. doi:doi:<https://doi.org/10.1080/10934529109375689>.
- Noever, D.A., Matsos, H.C., Looger, L.L., 1992. Bioconvective indicators in *tetrahymena*: Nickel and copper protection from cadmium poisoning. J. Environ. Sci. Health A 27, 403–417. doi:doi:<https://doi.org/10.1080/10934529209375735>.
- Omori, T., Habe, H., Yoshida, T., Horinouchi, M., Saiki, Y., Nojiri, H., 2003. Applied ecological microbiology. Shoko-do. (in Japanese).
- Omori, T., Nojiri, H., Horinouchi, M., Kasuga, K., 2002. Environmental Biotechnology. 3 ed., Shoko-do. (in Japanese).
- Pedley, T.J., Hill, N.A., Kessler, J.O., 1988. The growth of bioconvection patterns in a uniform suspension of gyrotactic micro-organisms. J. Fluid Mech. 195, 223–237. doi:doi:<https://doi.org/10.1017/s0022112088002393>.
- Pedley, T.J., Kessler, J.O., 1992. Hydrodynamic phenomena in suspensions of swimming microorganisms. Annu. Rev. Fluid Mech. 24, 313–358. doi:doi:<https://www.annualreviews.org/doi/abs/10.1146/annurev.fl.24.010192.001525>.
- Platt, J.R., 1961. Bioconvection patterns in cultures of free-swimming organisms. Science 133, 1766–1767. doi:doi:<https://doi.org/10.1126/science.133.3466.1766>.

- Shi, Q.H., Hamid, A., Khan, M.I., Kumar, R.N., Gowda, R.J.P., Prasannakumara, B.C., Shah, N.A., Khan, S.U., Chung, J.D., 2021. Numerical study of bio-convection flow of magneto-cross nanofluid containing gyrotactic microorganisms with activation energy. *Sci. Rep.* 11, 16030. doi:doi:<https://doi.org/10.1038/s41598-021-95587-2>.
- Tomita, H., Abe, K., 2000. Numerical simulation of pattern formation in the Bénard–Marangoni convection. *Phys. Fluids* 12, 1389–1400. doi:doi:<https://doi.org/10.1063/1.870390>.
- Tuval, I., Cisneros, L., Dombrowski, C., Wolgemuth, C.W., Kessler, J.O., Goldstein, R.E., 2005. Bacterial swimming and oxygen transport near contact lines. *Proc. Natl. Acad. Sci. U.S.A.* 102, 2277–2282. doi:doi:<https://doi.org/10.1073/pnas.0406724102>.
- Uddin, M.J., Kabir, M.N., Béq, O.A., 2016. Computational investigation of Stefan blowing and multiple-slip effects on buoyancy-driven bioconvection nanofluid flow with microorganisms. *Int. J. Heat Mass Transf.* 95, 116–130. doi:doi:<http://dx.doi.org/10.1016/j.ijheatmasstransfer.2015.11.015>.
- Van der Pol, L., Tramper, J., 1998. Shear sensitivity of animal cells from a culture–medium perspective. *Trends Biotechnol.* 16, 323–328. doi:doi:[https://doi.org/10.1016/S0167-7799\(98\)01209-8](https://doi.org/10.1016/S0167-7799(98)01209-8).
- Williams, C.R., Bees, M.A., 2011. A tale of three taxes: Photo-gyro-gravitactic bioconvection. *J. Exp. Biol.* 214, 2398–2408. doi:doi:<https://doi.org/10.1242/jeb.051094>.
- Yamamoto, Y., Okayama, T., Sato, K., Takaoki, T., 1992. Relation of pattern formation to external conditions in the flagellate, *chlamydomonas reinhardtii*. *Eur. J. Protistol.* 28, 415–420. doi:doi:[https://doi.org/10.1016/S0932-4739\(11\)80005-2](https://doi.org/10.1016/S0932-4739(11)80005-2).
- Yanaoka, H., Inamura, T., Suzuki, K., 2007. Numerical analysis of bioconvection generated by chemotactic bacteria. *JSME, Ser. B* 73, 575–580. doi:doi:<https://doi.org/10.1299/kikaib.73.575>. (in Japanese).
- Yanaoka, H., Inamura, T., Suzuki, K., 2008. Three dimensional numerical analysis of bioconvection generated by chemotactic bacteria. *JSME, Ser. B* 74, 135–141. doi:doi:<https://doi.org/10.1299/kikaib.74.135>. (in Japanese).
- Zadeha, S.M.H., Mehryanb, S., Sheremetc, M.A., Izadid, M., Ghodrate, M., 2020. Numerical study of mixed bio-convection associated with a micropolar fluid. *Therm. Sci. Eng. Prog.* 18, 100539. doi:doi:<https://doi.org/10.1016/j.tsep.2020.100539>.